Nuclear Halo Effect and Field Size Factor for Pencil-Beam Scanning Proton Therapy

by

Atdhe Beqiri

A Thesis Submitted to the Faculty

of Charles E. Schmidt College of Science

In Partial Fulfillment of the Requirements for the Degree of

Professional Science Master

Florida Atlantic University

Boca Raton, FL

August 2021

Nuclear Halo Effect and Field Size Factor for

Pencil-Beam Scanning Proton Therapy

by

Atdhe Beqiri

This thesis was prepared under the direction of the candidate's thesis co-advisors, Dr. Wazir Muhammad, Department of Physics, and Dr. Charles Shang, Department of Physics, and has been approved by all members of the supervisory committee. It was submitted to the faculty of the Charles E. Schmidt College of Science and was accepted in partial fulfillment of the requirements for the degree of Professional Science Master.

SUPERVISORY COMMITTEE:

Charles Shang
Charles Shang (Jul 22, 2021 09:22 EDT)

Charles Shang, MB, MS, DABR
Thesis Co-Advisor

WAZIR MUHAMMAD
WAZIR MUHAMMAD (Jul 24, 2021 01:16 EDT)

Wazir Muhammad, Ph.D.
Thesis Co-Advisor

Theodora Leventouri
Theodora Leventouri (Jul 24, 2021 02:53 EDT)

Theodora Leventouri, Ph.D.

Luc Wille (Jul 28, 2021 10:57 EDT)

Luc Wille, Ph.D.
Chair, Department of Physics

Teresa Wilcox

Teresa Wilcox, Ph.D.
Interim Dean, Charles E. Schmidt College of Science

Robert W. Stackman Jr., Ph.D.
Dean, Graduate College

July 29, 2021

Date

Acknowledgments

Firstly, I thank my Thesis Advisor, Dr. Charles Shang for his support, guidance, innovative ideas, constant encouragement, optimism, willingness to discuss science at any time and for giving me the opportunity to join his team during this project, which provided me with such valuable knowledge and experience in Proton Therapy.

I would like to thank my advisory committee: Dr. Wazir Muhammed for his support and Dr. Theodora Leventouri, for all her support and guidance for my personal and professional goals.

I also thank the physicists at the South Florida Proton Therapy Institute: Grant Evans, Mushfiqur Rahman and Maxwell Kassel for their support with Eclipse planning and technical information during this project.

Last, but not least, I want to sincerely thank my family, for their endless love and encouragement, and all my friends and loved ones.

Abstract

Author: Atdhe Beqiri

Title: Nuclear Halo Effect and Field Size Factor for Pencil-Beam Scanning Proton Therapy

Institution: Florida Atlantic University

Thesis Advisor: Charles Shang, MB, MS, DABR

Thesis Co-Advisor: Wazir Muhammad, Ph.D.

Degree: Professional Science Master

Year: 2021

In proton therapy systems with pencil-beam scanning, output of Halo effect is not necessarily included in Treatment Planning System (TPS). Halo effect (low-intensity tail) can significantly affect a patient's dose distribution. The output of this dose depends on the field size being irradiated. Although much research has been made to investigate such relation to the field size, the number of reports on dose calculations including the halo effect is small. In this work we have investigated the Halo effect, including field size factor, target depth factor, and air gaps with a range shifter for a Varian ProBeam.

Dose calculations created on the Eclipse Treatment Planning System (vs15.6 TPS) are compared with plane-parallel ionization chambers (PTW Octavius 1500) measurements using PCS and AcurosPT MC model in different isocenters: 5cm, 10cm, and 20cm.

We find that in AcurosPT algorithm deviations range between -7.53% (for 2cm field in 25cm air gap with range shifter) up to +7.40% (for 20cm field in 15cm air gap with range shifter). Whereas, in PCS algorithm the deviations are -2.07% (for 20x20cm field in open conditions) to -6.29% (for 20x20cm field in 25cm air gap with range shifter).

For small fields (2cm) and in deeper depth the AcurosPT output is 4.11% less than the PCS, and in shallower depth PCS delivers up to 8.07% more dose than AcurosPT.

For big fields (10cm and 20cm) in both deep and shallower depth the AcurosPT delivers more dose than PCS. In deeper depth targets (20cm field) the difference is 11.09% and in shallower depth (15cm air gap) is 12.94%.

Thus, as the field size increases the discrepancies tend to grow. These discrepancies intensify, especially when we use a range shifter with higher air gaps of 15cm and 25cm.

This data could be used in proton clinics using pencil beam scanning to have a better understanding in deviations of dose calculations and dose delivery.

.

Nuclear Halo Effect and Field Size Factor for

Pencil-Beam Scanning Proton Therapy

List of Tables

List of Figures

Chapter 1: Introduction

When many abnormal cells divide in uncontrollable way and end up killing normal cell/tissues of the body, then this is referred as Cancer. Technological improvement for the past decades in diagnostics and treatment are the reason that the survival rates are constantly improving. One of the methods to control or destroy cancer cells is through radiation therapy, which it can be external or internal. External beam therapy is also known as radiation therapy, and it uses high energy particles like photons, or protons. Internal radiotherapy is called Brachytherapy, where the radiation source (iodine-125 or cesium-131) is placed inside the body where the tumor is located. In comparison with conventional radiotherapy (uses photo beams) proton beam therapy may offer dosimetric advantages. The advantages come from protons being able to deliver higher proportion of their dose to the target, a characteristic known as Bragg Peak, and having minimal exit dose (Fig.1.1).

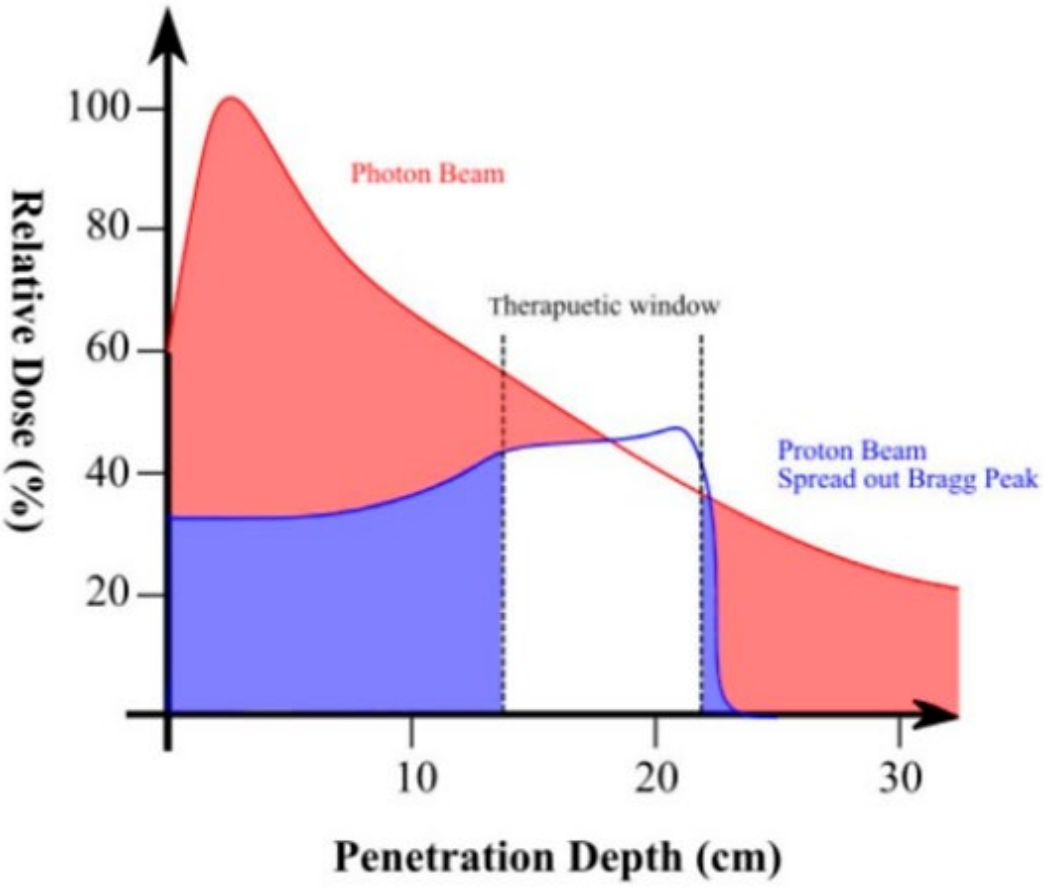

Fig.1.1. Spread out Bragg Peak of proton therapy (blue) compared to photon therapy (red). The shaded areas represent relative dose to normal tissue. This figure is adapted from [1].

The advantages of proton pencil scanning (PBS) like conformal dose distribution with minimal exit dose is also associated with dose calculations uncertainties.

In this study we will focus in determining the uncertainties related to nuclear halo effect and field size factor.

1.1 Elementary Particles

Matter is what makes everything in universe. Matter itself is made of smaller particles which interacts with each other via four forces of nature. These fundamental particles can be classified in two categories: Fermions (constituent of matter) and Bosons (force carriers). The main difference between them is the spin integral.

Bosons include γ photon, Z boson, W boson, ang g gluon.

Fermions have a spin in odd half integer quantum units of angular momentum (1/2, 3/2, …), whereas bosons have a spin of an integer number (1, 2, 3, …).

There are two types of fermions: Quarks and Leptons.

Leptons have a spin 1/2 and they are defined in pairs: electron (e^-) and the electron neutrino (ν_e), muon (μ^-) and the muon neutrino (ν_μ), and tau (τ), and its tau neutrino (ν_τ).

Quarks are the building blocks of heavier particles called Hadrons. Hadrons include baryons (proton and neutron – half integral spins) and mesons (integer spin). Six different quarks exist: Up (u), Down (d), Charm (c), Strange (s), Top (t), and Bottom (b). Protons, neutrons and are made of three quarks: uud and ddu respectively.

Gluons (the messenger particle) is the particle which keeps the quarks together.[2]

1.2 *Forces in nature*

Interactions between various types of particles are what defines the forces in nature. There are four fundamental forces in nature: strong nuclear force, electromagnetic force, weak force, and gravitational force. The main characteristics of these forces are their strength and their range.

Classification of these forces regarding their strength is based in the strength normalization of 1 for the strong force:

1. Strong Nuclear force – with relative strength of 1.
2. Electromagnetic (EM) force – 1 with relative strength of 1/137.
3. Weak force – with relative strength of 10^{-6}.
4. Gravitational force – with relative strength of 10^{-39}.

Range of this forces it classifies them in two groups:

a. Infinite range – EM and Gravitational forces.

b. Short range – Strong and Weak forces (few femtometers). [3]

1.3 Radiation Physics

The four fundamental forces of nature are the reason that everything in universe is in constant motion. Strong and weak forces are responsible for the motion of small particles (quantum world) while the electromagnetic and gravitational forces are responsible for the motion of larger object. While in motion these particles have energy and mass. They also travel in form of waves (i.e light waves, heat rays etc).

Thus, this particles or energy that travel from a source through space or a medium is referred to as *radiation*. A form of wave energy in motion is called Electromagnetic Radiation (EMR). Electromagnetic radiation consists of small "packages" which carry the energy – photons. Photons are massless and they travel with a speed of 2.998×10^8 m/s. This is known as speed of light (c). Characteristic of EMR is depended on the wavelength. Frequency (λ) and wavelength (f) are inversely proportional. [4]

$$c = \lambda v \qquad (1)$$

Other types of small particles (electron, alpha particles, protons) can carry the energy through the medium and this is particulate radiation.

1.4 Radiation Classes

The energy carried by different particles can lead to excitation (moving an electron from an inner shell to outer shell) or ionization (remove the electron completely from the atom). Hence, we can categorize radiation in two groups:

a) Non – ionizing radiation.

b) Ionizing radiation.

a). Non – ionizing radiation refers to radiation which does not have the minimum energy to ionize atoms or molecules of the medium/absorber. Types of non – ionizing radiations are UV light, visible light, microwaves, and radio waves.

b) Ionizing radiation carries enough energy to ionize the atoms or molecules of the medium/absorber. [3]

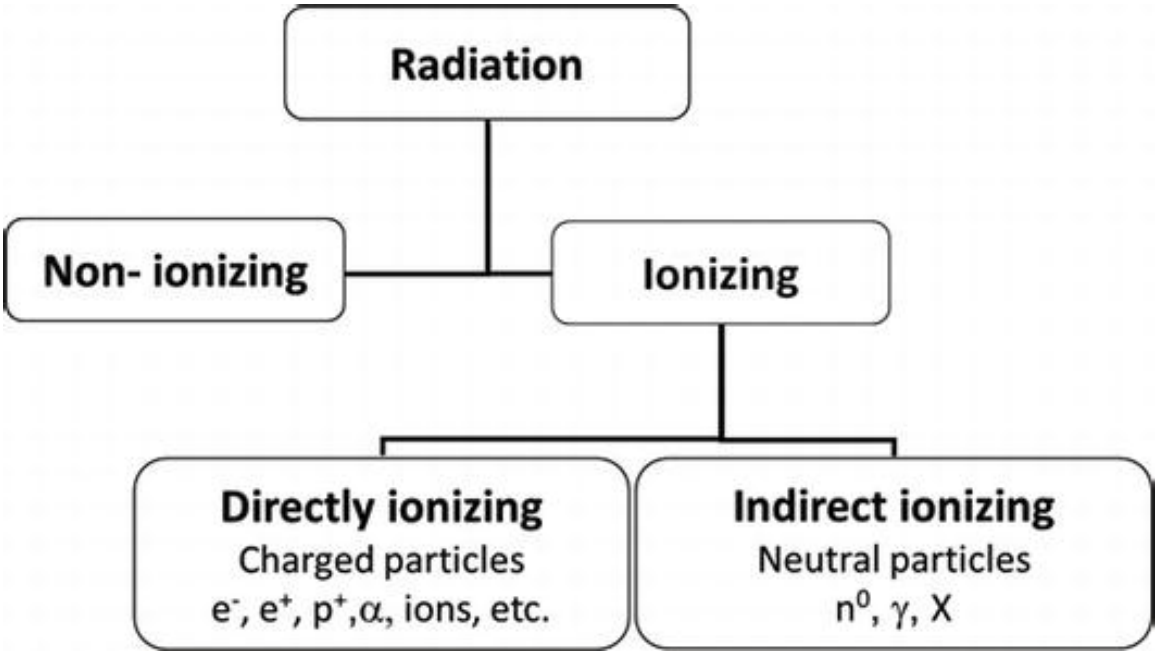

Fig.1.2. Classification of radiations. This figure is adapted from [5].

1.4.1 Ionizing Radiation

Ionizing radiation can be classified depending on the density of the ionization that it produces in the medium/absorber in two groups:

i. Directly ionizing radiation.

ii. Indirectly ionizing radiation.

(i) In directly ionizing radiation the energy from charged particles (electrons, protons, alpha particles, heavy ions) is transferred to the medium/absorber in a direct one-step process (Coulomb interaction takes place between charged particles and orbital electrons of the absorber).

(ii) Indirectly ionizing radiation includes neutral carriers such as photons (x-ray and γ rays) and neutrons. This is a twostep process where first the charged particles are released in the medium/absorber and after that the released charged particles releases their energy in the medium/absorber through Coulomb interactions.[3]

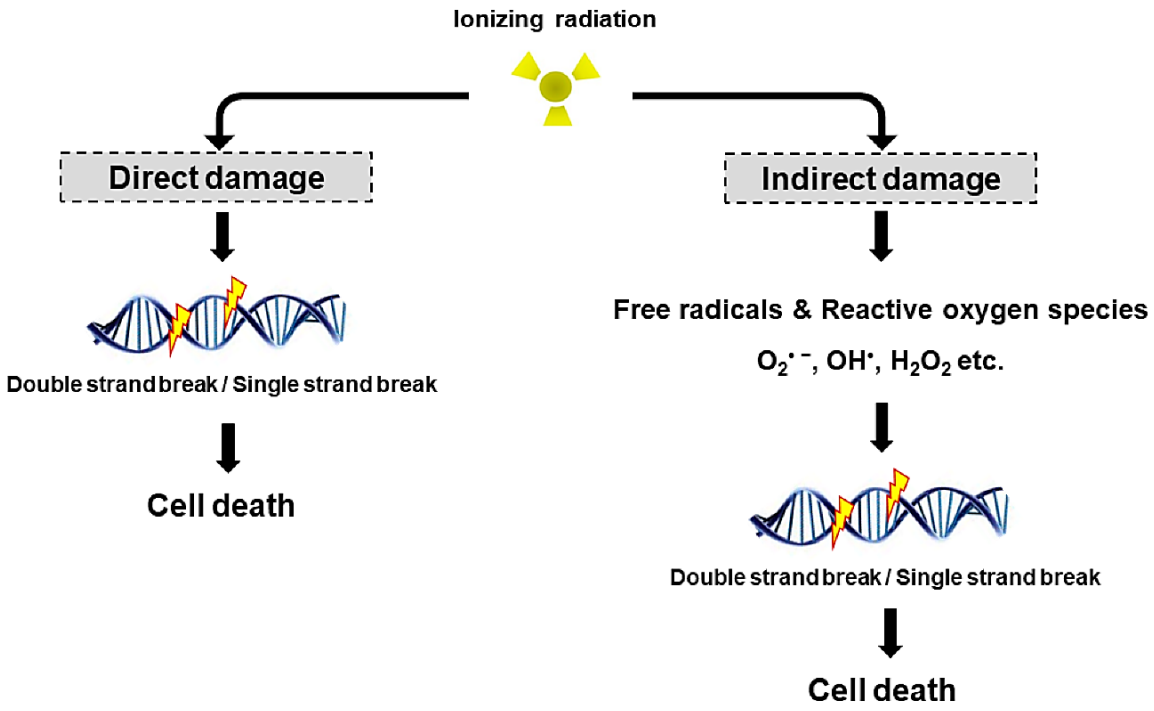

Fig.1.3. Direct and indirect DNA damage by ionizing radiation.

This figure is adapted from [6].

Chapter 2: Physics of Proton

2.1 Particulate Radiation

Particulate radiation is referred to the charged particles which have mass, energy and electric charge. These particles are electrons, alpha particles, π-mesons, heavy charged ions and protons. Protons together with neutrons create the nucleus of an atom. Protons are positively charged particles 1.602×10^{-19} C with mass of 1836 times the mass of an electron and, have a half-life of 10^{35} years. The rest mass of a proton is 1.67262×10^{-27} kg (938.27 MeV/c^2).
Radiation interacting with matter can be either scattered or absorbed [7]. Protons interact with matter/tissue in a different way than photons of electrons. They tend to travel in straight lines and produce long tracks with the energy concentrated closer to the track of the primary particle, while photons or electrons tend to scatter more easily and produce a more uniform distribution of energy transfers.[8]

2.2 Proton Interactions

As proton travel through matter, it might interact by electronic or nuclear reaction. The Coulomb electronic interactions are ionization and excitation of atomic electrons whereas the nuclear interactions are Coulomb scattering, elastic collision, and non-elastic nuclear collision.

2.2.1 Energy Loss of Protons

Protons once they enter the absorber, they lose their energy by Coulomb interactions with the outer shell electrons which causes excitation (soft collision) or ionization (hard collision - delta (δ) ray production) (Fig.2.1). Inelastic collision may occur without loss of energy in this region. The deflection of proton at this area is insignificant because the energy lose per interaction is small. The range of secondary electrons is less than 1 mm and most of the dose is absorbed locally. Energy of the protons diminishes as the proton travels deeper in the tissue so that the number of ionizations events rapidly increase and reaching its peak known as a Bragg peak (Fig.2.3). After the Bragg peak the number of ionizations decreases to zero. Linear stopping power is the average energy loss per distance (Fig.2.3):

$$S = -\frac{dE}{dx} \tag{2}$$

Linear stopping power can be expressed in terms of the quantity called “mass stopping power”. Mass stopping power is energy loss per unit path length in g/cm^2 (unit is MeV-cm^2/g).

$$\frac{S}{\rho} = -\frac{dE}{dx} \tag{3}$$

$\frac{S}{\rho}$ is the stopping power, E is the energy loss per distance x.

Mass stopping power can be explained by Bloch-Bethe formula who considers relativistic effect (at low proton energy) and quantum mechanical effect (at high proton energy) [2]:

$$\frac{S}{\rho} = 4\pi N_A r_e^2 m_e c^2 \left(\frac{Z}{A}\right)\left(\frac{z^2}{\beta^2}\right)\left[\ln\frac{2m_e c^2\gamma^2\beta^2}{I} - \beta^2 - \frac{\delta}{2} - \frac{C}{Z}\right] \quad (4)$$

Z – is the atomic number of the absorbing material,
N_A – is Avogadro's number,
r_e – is the classical electron radius,
A – is the atomic weight of the absorbing material, and
z – is the charge of the particle (equal to 1 for a proton).
β – is v/c where v is the particle's velocity and c is the speed of light,
m_e – is the mass of an electron,
γ – is equal to $(1- \beta^2)^{1/2}$,
I – is the mean excitation potential of the absorbing material,
C – is the shell correction factor, and δ – is the density correction factor.

Therefore, the low atomic number (Z) materials have the greater mass stopping power than high-Z materials (i.e.1 MeV proton is 25.4 MeV/kg/m^2 in water and 6.39 MeV/kg/m^2 in lead). High Z materials scatter the proton at a larger angle without much energy loss so that those materials are used to spread out the beam. [9]

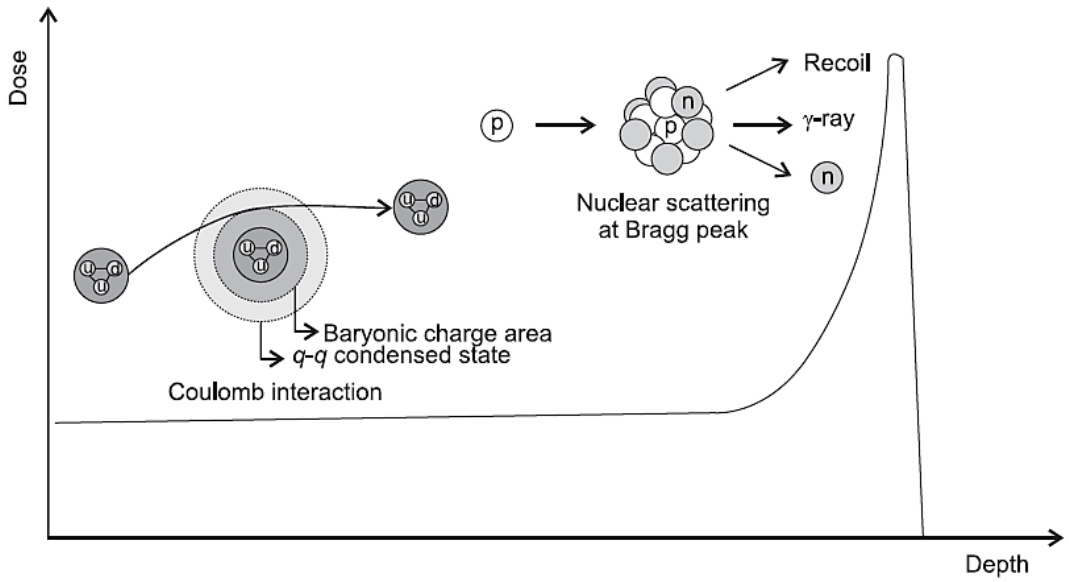

Fig.2.1. Interaction of protons. The Coulomb interaction slows the velocity of protons before Bragg peak. As the stopping power increases, the energy of proton lowers at the Bragg peak where the proton interacts with nucleus to emit secondary neutron and γ - rays. This figure is adapted from [2].

2.2.2 Proton Range

The distance that a charged particle travels before it comes to rest is called Range. Range is expressed in gcm^{-2}, like mass stopping power, range it applied to all materials of similar atomic composition. Range straggling is the distribution of ranges resulting from particles of a single incident energy and due to that range is an average quantity defined for a beam rather than for individual particles and it is defined in terms of fluence as the depth at which 50%, 80% or 90% of the incident primary protons in a beam have come to rest. In clinical settings we define range at the 90% (R_{90}) distal dose falloff position. [10] Range

straggling follows a normal distribution and is approximately a constant fraction of proton range. Because the protons are deflected from the straight trajectory as they travel in the absorber, we must calculate the true trajectory. Bethe and Bloch theoretical calculation is given by proton continuous-slowing-down-approximation (CSDA) range:

$$R_{CSDA} = -\int_{E_0}^{0} \left(\frac{dx}{dE}\right) dE \quad (5)$$

Bragg–Klemann rule can also be used to calculate proton range [11]:

$$R_{CSDA} = \alpha E_0^p \quad (6)$$

α – is a material-dependent constant.
E_0 – is the initial energy of the proton beam.
p – the dependence of the proton energy.

We can see that with an increase in the proton energy their ranges increase. Therefore, proton ranges of 26-38 cm in tissue correspond to proton energies of 200 MeV to 250 MeV.[12].

Although, the determination of the proton range has many uncertainties. Those uncertainties are result of Coulomb scattering, CT conversion of HU to stopping power and CT resolution, and biological effects. [13]

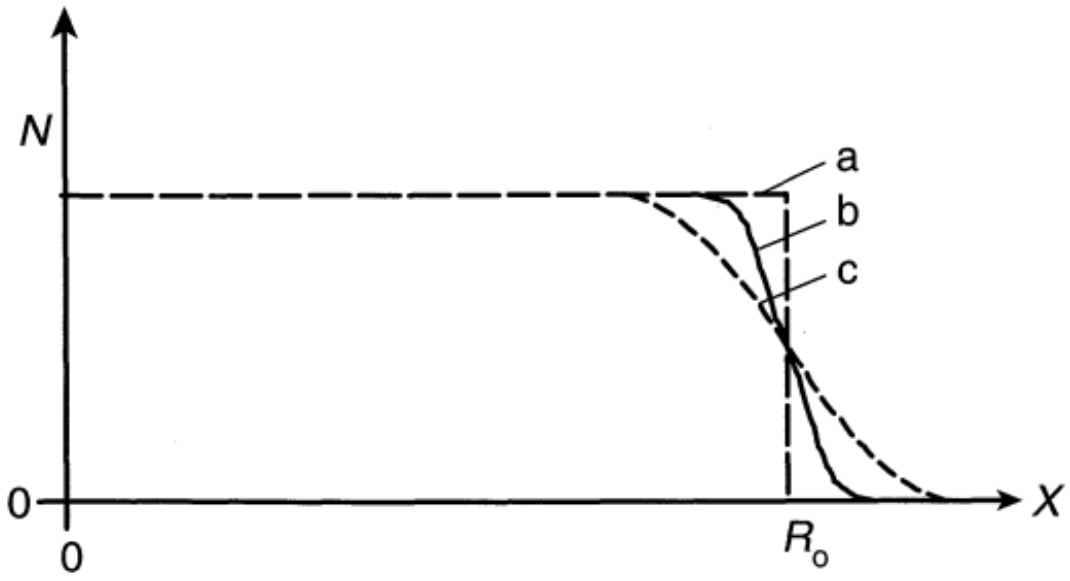

Fig.2.2. Penetration curves. a: No energy loss fluctuations,

b: Elastic electron-proton interactions, c: Curve b + inelastic interactions.

This figure is adapted from [14].

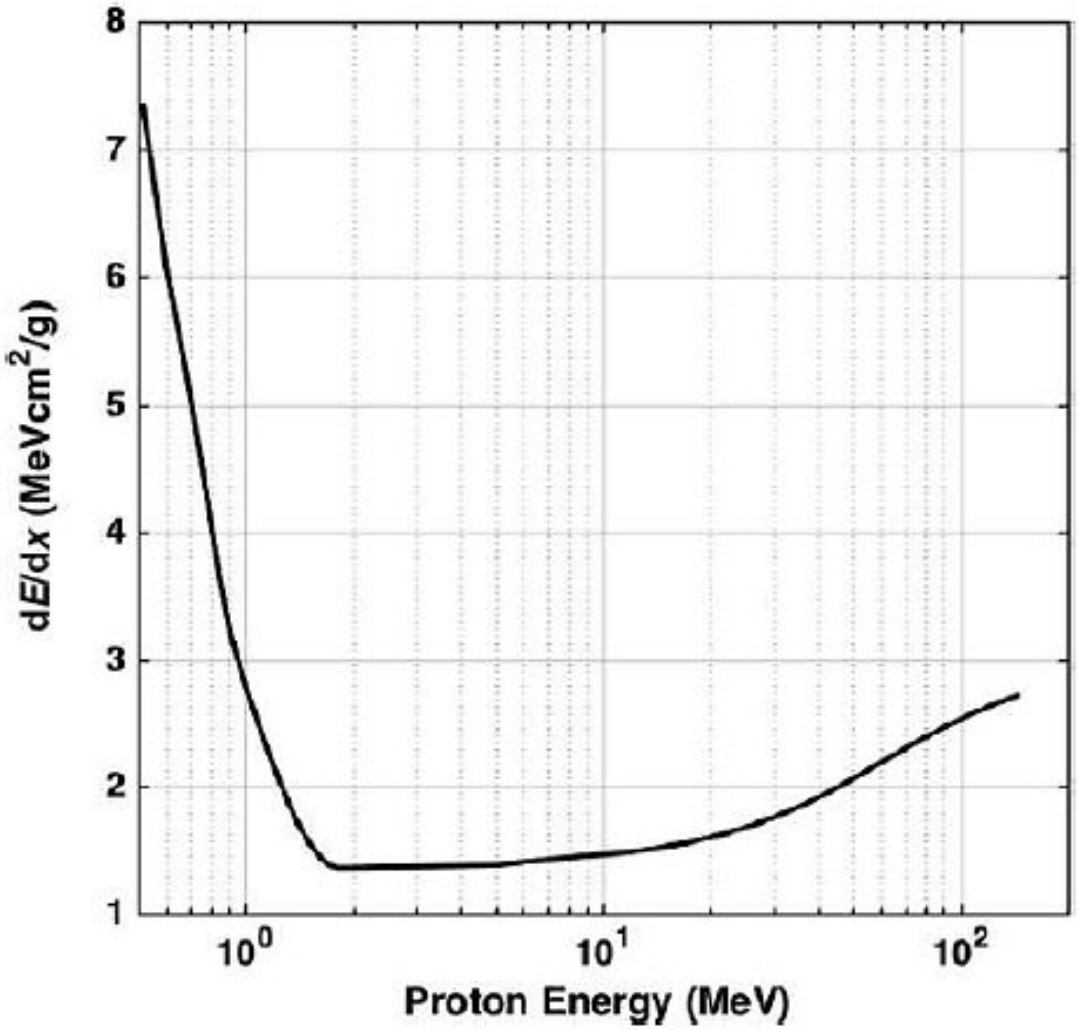

Fig. 2.3. The energy loss (*dE*/*dx*) as a function of proton kinetic energy for protons traveling through water. Most importantly, the energy loss increases rapidly as the proton slows in the medium. This rapid energy loss gives rise to the Bragg peak. This figure is adapted from [15].

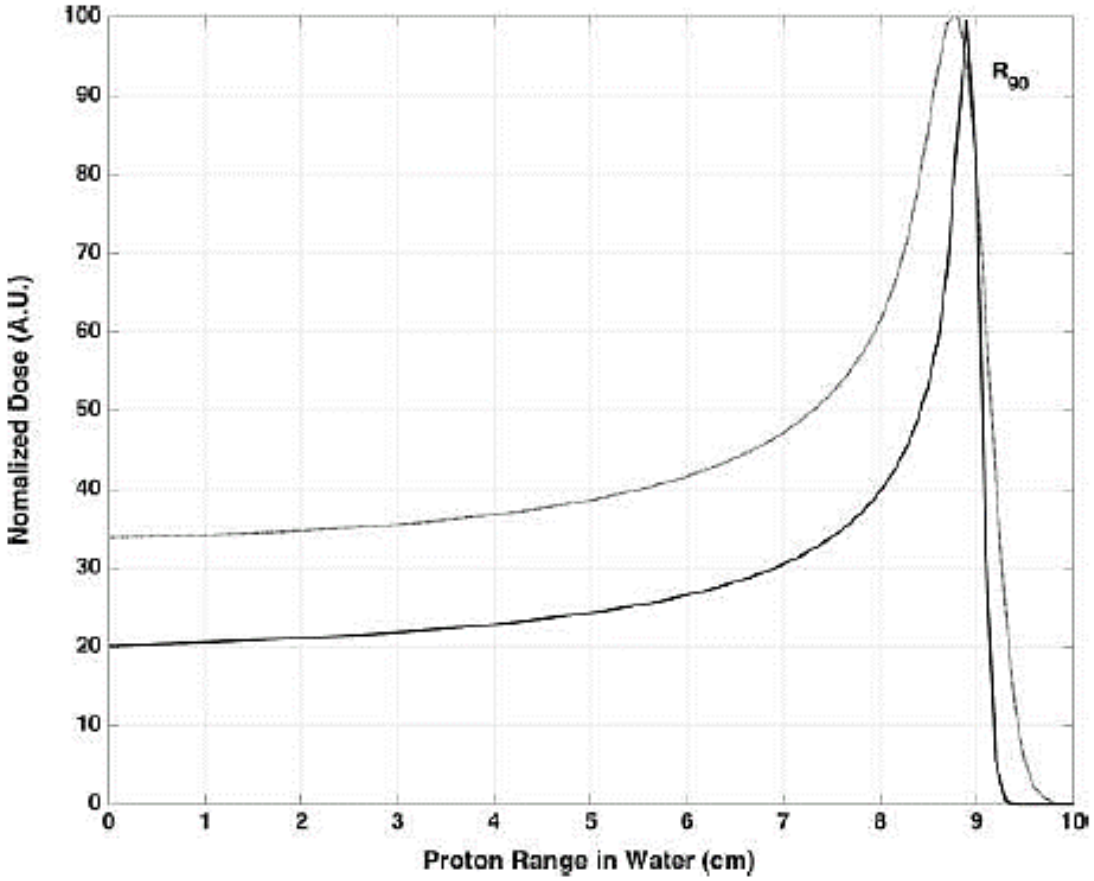

Fig.2.4. The proton energy deposited into the medium (water) as a function of proton range. The *dotted line* represents the effects of proton energy straggling as the protons stochastically interact with the medium. The R_{90} range is labeled. This figure is adapted from [15].

2.2.3 Proton Scattering

The shape and width of the angular distribution of the scattered protons is calculated by the scattering theory. In the region of interest (proton energy ≤ 300 MeV) elastic interaction of the proton with the Coulomb fields of the nucleus and

the orbiting electrons dominates the scattering process. The main contribution results from Coulomb interaction of the proton with the nucleus. The influence of inelastic nuclear interactions of the proton is treated separately because:

1. The interaction probability decreases rapidly with increasing proton energy, consequently it has little influence on the region of main interest, the Bragg peak.

2. The scattering angles and the energy losses involved are so large, that very few, inelastically scattered protons will reach the region of interest, the target volume.[14]

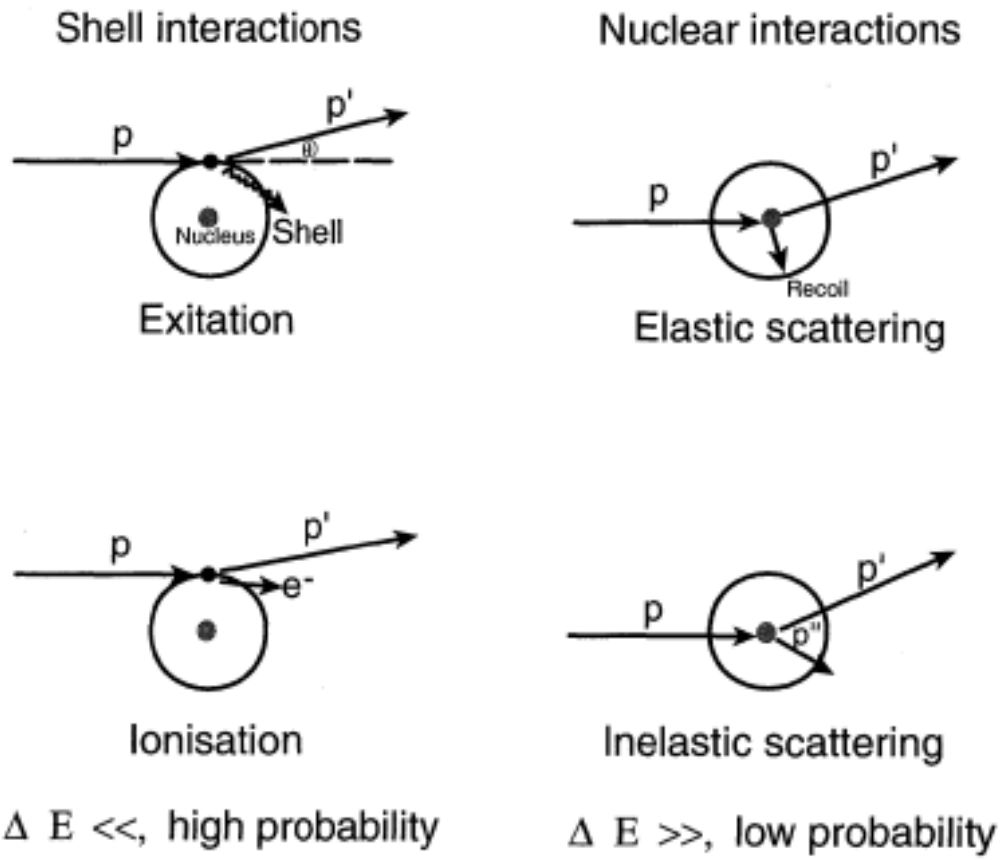

Fig.2.5. Simplified schematics of the energy loss processes encountered by protons in the energy range of interest for radiotherapy. This figure is adapted from [16].

It is called elastic scattering, because:

I. The incident particle is also the exiting particle.

II. The energy loss of the incident proton during each single scattering event is very small.

III. The total kinetic energy of all participants is conserved.

The phenomenon of Multiple Coulomb Scattering (MCS) is a result of numerous very small angular deflections. For thin layers of absorbers, the shape is Gaussian whereas for thick layers it deviates significantly from a Gaussian. The relative contributions to its 'tail' are especially enhanced. [14]

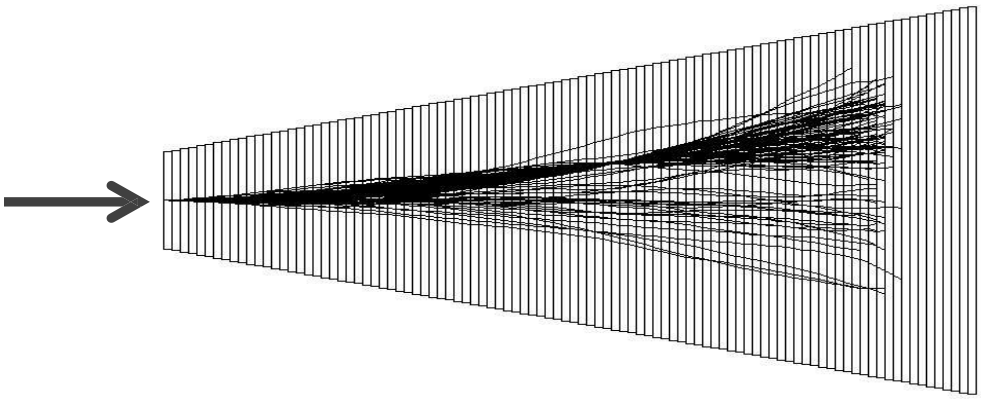

Fig.2.6. Mono-energetic incident protons (Transverse scale greatly exaggerated). This figure is adapted from [17].

Multiple Coulomb Scattering angular distribution for small angles was presented by Molière. Gaussian and non-Gaussian broad tails regions of the angular distribution were included in his calculations.

$$f(\theta, d) = \frac{1}{4\pi\theta_M^2}\left[f^{(0)}(\theta') + \frac{f^{(1)}(\theta^1)}{B} + \frac{f^{(2)}(\theta')}{B^2} \ldots\right] \quad (7)$$

θ – proton angle with respect to the forward direction, in radian
d – penetrated thickness, in g/cm^2
θ_M^2 – characteristic multiple scattering angle, in radian
$\theta_M^2 = 1.56\ d\ B\ Z^2 / [2A\ (p\nu)]$

B – a quantity depending on the number of collisions for the proton
Z, A – atomic number, relative atomic weight of scatterer
p, ν – momentum, speed of proton

However, corrections for the large-angle scatter must be included.[18] One of the approximations to the Molière theory for thin scatter was conducted by Highland (1975/79).

$$\theta_{approx} = \frac{14.1}{p\nu}\left(\frac{d}{1-R}\right)^{-\frac{1}{2}}(1 + \varepsilon) \quad (8)$$

L_R – radiation length of scattering material, in g/cm^2 (LR enters the equation only because it is convenient for the computation).

The correction term ε (expressed in radian) is:

$$\varepsilon = \frac{1}{9} lg\left(\frac{L}{L_R}\right) \quad (9)$$

The accuracy of (8) is better than 5% for d ≥ 0.001 R. [14]

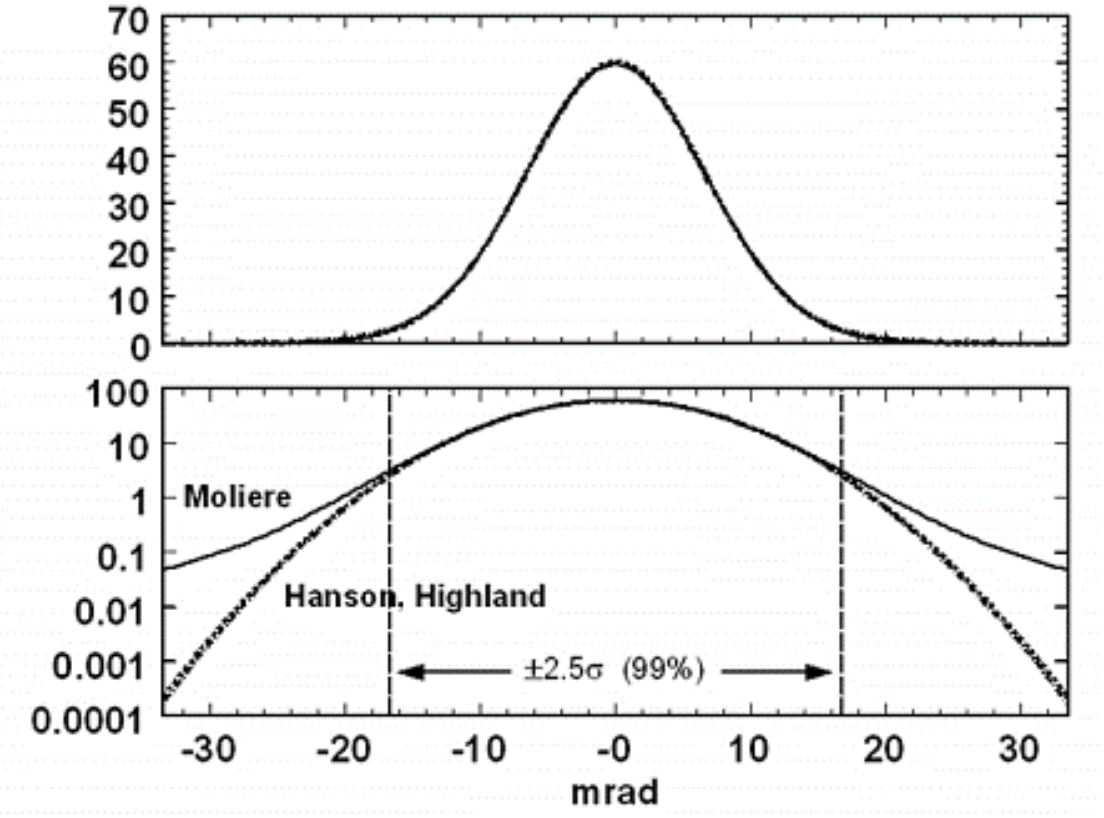

Fig.2.7. Angular distributions for 158.6 MeV protons traversing 1 cm of water. This figure is adapted from [17].

2.2.4 Proton Nuclear Interaction

Protons in the absorbing material undergo electromagnetic (EM) interactions with electrons (which slow them down) and with nuclei (which scatter them). For a 160 MeV proton in water, it has been shown that around 23% have a head-on collision with an atomic nucleus. After this collision, the energy of proton is way less, it has a large angle to the beam, and it is accompanied by other charged and neutral secondaries and a residual nucleus. ICRU Report 63, ‘Nuclear Data

for Neutron and Proton Radiotherapy and for Radiation Protection' (2000), defines the possible proton nuclear reactions [19]:

- *Elastic* nuclear reaction is a reaction in which the incident projectile scatters off the target nucleus, with the total kinetic energy being conserved (the internal state of the target nucleus and of the projectile are unchanged by the reaction)
- *Nonelastic* nuclear reaction is a general term referring to nuclear interactions that are not elastic (*i.e*., kinetic energy is not conserved). For instance, the target nucleus may undergo breakup, it may be excited into a higher quantum state, or a particle transfer reaction may occur.
- *Inelastic* refers to a specific type of nonelastic reaction in which the kinetic energy is not conserved, but the final nucleus is the same as the bombarded nucleus [20].

Table 2.1. Equations of some of the most common elastic, nonelastic and inelastic nuclear reactions in proton therapy.

Elastic	Nonelastic	Inelastic
1. $p + O_8^{16} \Rightarrow p + O_8^{16}$ or O_8^{16} (*p, p*) O_8^{16}	1. $p + O_8^{16} \overset{d}{\Rightarrow} p + p + N_7^{15}$ or O_8^{16} (*p, 2p*) N_7^{15} 2. $p + O_8^{16} \Rightarrow p + n + O_8^{15}$ 3. $p + O_8^{16} \Rightarrow n + F_9^{16}$	1. $p + O_8^{16} \Rightarrow p + {}^{16}O^{*}$ or ^{16}O (*p, p*) $^{16}O^{*}$ (* denotes an exited state)

Primary particles are protons when they slow down and stop in matter.

Secondary Particles are created by Nonelastic (at therapy energies: protons, neutrons, γ rays, α particles and recoiling residual nucleus) and inelastic nuclear reactions.

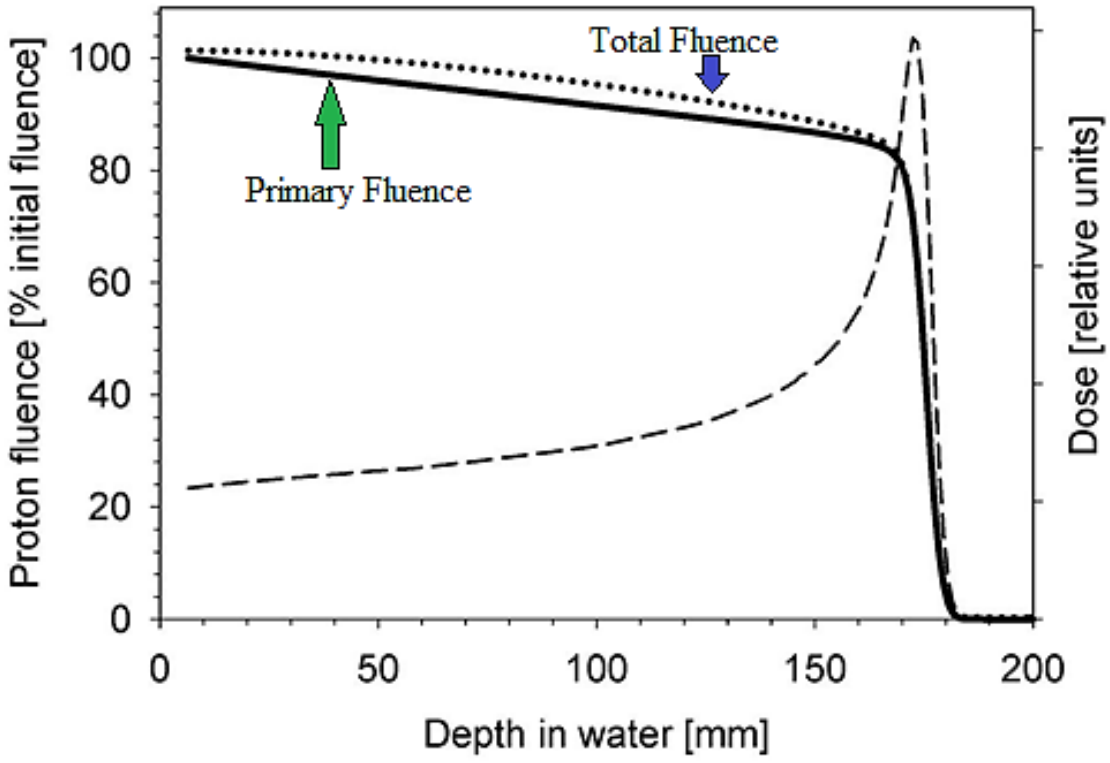

Fig.2.8. Dose by Nuclear Interactions. This figure is adapted from [21].

2.3 Proton Beam Halo and Field Size Factor

Another important interaction that protons go through in matter is single hard scatters. The hard scatter interaction is rare compared with multiple collision with atomic electrons and atomic nuclei and that is the reason why we do not treat them as correction. In this process occasionally by nuclei or their constituents they throw dose out to large distances from the beam [17]. In single hard collision we have the effect what Pedroni [22] called the nuclear halo. Thus, *the halo* is the surrounding dose resulting from charged secondary particles (originated in

non-elastic nuclear interactions in a phantom or patient), then we have *the core* which is the central dose due to primary protons and *the aura,* which is a very large region of dose from neutral secondaries (fig.2.9). [17] Separation between the halo and main core of the beam it's not clearly defined. Increased population of the outer part of the beam is a general characteristic of the halo beam. In coordinate space, beam-profile parameter can be used to describe that. Beam-profile for the transverse x-coordinate can be defined as:

$$h_x = \langle x^4 \rangle \, / \, \langle x^2 \rangle^2 - 2 \tag{10}$$

Beam-profile for an ellipsoidal beam in the x-coordinate is:

$$h_x = \langle x^4 \rangle \, / \, \langle x^2 \rangle^2 - 15/7 \tag{11}$$

Similarly, for the h_y and h_z in the other directions. Beam-profile parameter increases as the population of the particle with large transverse amplitudes increases (halo develops in beam). [23] The halo radius is roughly one-third the beam range. Even though, halo for an individual pencil beam is orders of magnitude beam's smaller than the dose in the central axis, because of combinations (overlapping of low dose tails) effect of a large number of pencil beams in the radiation field, up to 15% of the total dose can be attributed to the beam halo [22]. Hence, for a small area in the center of a given field, the dose

delivered is influenced by the irradiation of the field size. Thus, halo effect depending on the filed size factor, may deliver wanted or unwanted dose. [17]

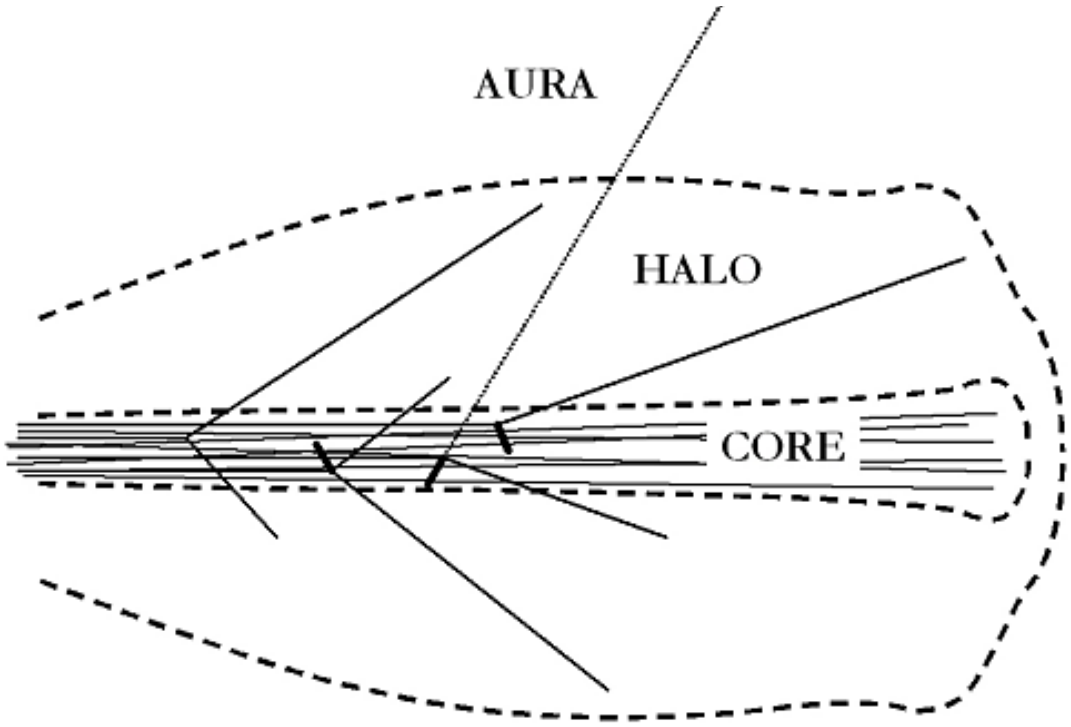

Fig.2.9. Core, halo and aura with reactions. From the left: $^{1}H(p,p)p$ (Hard scattering on free hydrogen -elastic); $^{16}O(p,2p)^{15}N$ (Quasi-elastic p-p scattering – nonelastic); $16O(p,pn)^{15}O$ (Quasi-elastic proton neutron) and $^{16}O(p,p)^{16}O$ (elastic proton-nucleus -scattering to small angles is electromagnetic). Recoil nuclei ranges are exaggerated. The dashed lines are 10% and 0.01% isodoses drawn to scale. This figure is adapted from [18].

2.4 The Bragg Peak (BP)

Proton interaction that we discussed they combine in the curve known as Bragg Peak. The dose deposited by a beam of monoenergetic protons increases slowly with depth but reaches a sharp maximum near the end of the particles' range in the Bragg peak (fig.2.10). [24]

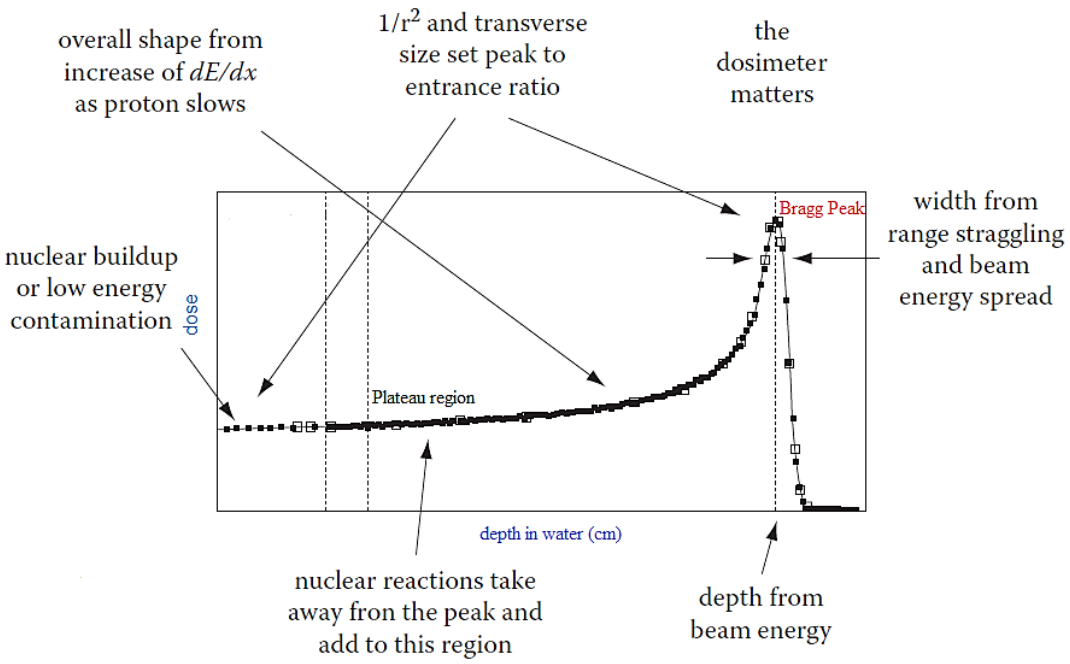

Fig.2.10. Characteristics of the Bragg Peak. This figure is adapted from [16].

From the figure 2.10 we can see that the shape of the Bragg peak depends on the fundamental variation of stopping power with energy, the transverse size of the beam, range straggling, beam energy spread, nuclear interactions, low energy contamination, effective source distance, and the dosimeter used in the measurement.

- The increase of dE/dx as the proton slows down causes the overall upwards sweep.
- The depth of penetration (measured by d_{80}) increases with beam energy.
- The width of the peak is the quadratic sum of range straggling and beam energy spread. Straggling width relative to range is almost independent of energy so absolute straggling width increases with energy. Therefore, the BP gets wider.[16]

$$d_{20} - d_{80} = 1.3 \times (\sigma_{RS}^2 - \sigma_{beam}^2)^{1/2} \quad (12)$$

- The overall shape depends on the beam's transverse size. The fluence on the central axis of a pencil beam decreases with depth because of out-scattering of the protons. The dose on axis (fluence × stopping power) therefore goes down; the Bragg peak vanishes. In a broad beam the axial fluence is restored by in-scattering from neighboring pencils (*transverse equilibrium*).
- Non-elastic nuclear reactions lower the BP move dose from the peak upstream.
- A short effective source distance reduces the peak/entrance ratio. [25]

2.5 Relative Biological Effectiveness – RBE

The form of a dose-response curve depends on the type of cells irradiated, the type and energy of radiation used, and the biological end point studied. If a dose D’ of a given

radiation type produces the same biological end point in a given experiment as a dose D of our reference radiation, we can define a quantity called the relative biological effectiveness (RBE) [26]

$$RBE = \frac{D}{D'} \tag{13}$$

Factors that RBE varies are LET, dose and endpoints and tissue (α/β ratio). RBE will increase with an increase in LET, reaching a maximum and then decreasing. In proton radiation therapy there are uncertainties in the RBE value for any human tissue to propose RBE values specific for tissue, dose/fraction, proton energy, etc. Per clinical data and experimental results, AAPM and other national organizations elected an average RBE value of 1.1 for current proton dose clinical scaling factor. In a treatment planning, especially for single field plans or for an end of range in or close to a critical structure there is a local “hot region” over the terminal few millimeters of the SOBP and an extension of the biologically effective range needs to be considered.[27]

2.6 Proton Beam Delivery – Pencil Beam Scanning

One of the goals of the radiation treatment is that all tissue element in the target volume should receive the same amount of dose. In proton therapy the energy of protons needs to be adjusted before dose in depth gets distributed in the patients because protons after coming out of the accelerator, they have a lateral spread out (few mm). This adjustment can be done in two ways:

1. Passive Scattering
2. Active Scanning – Pencil Beam Scanning

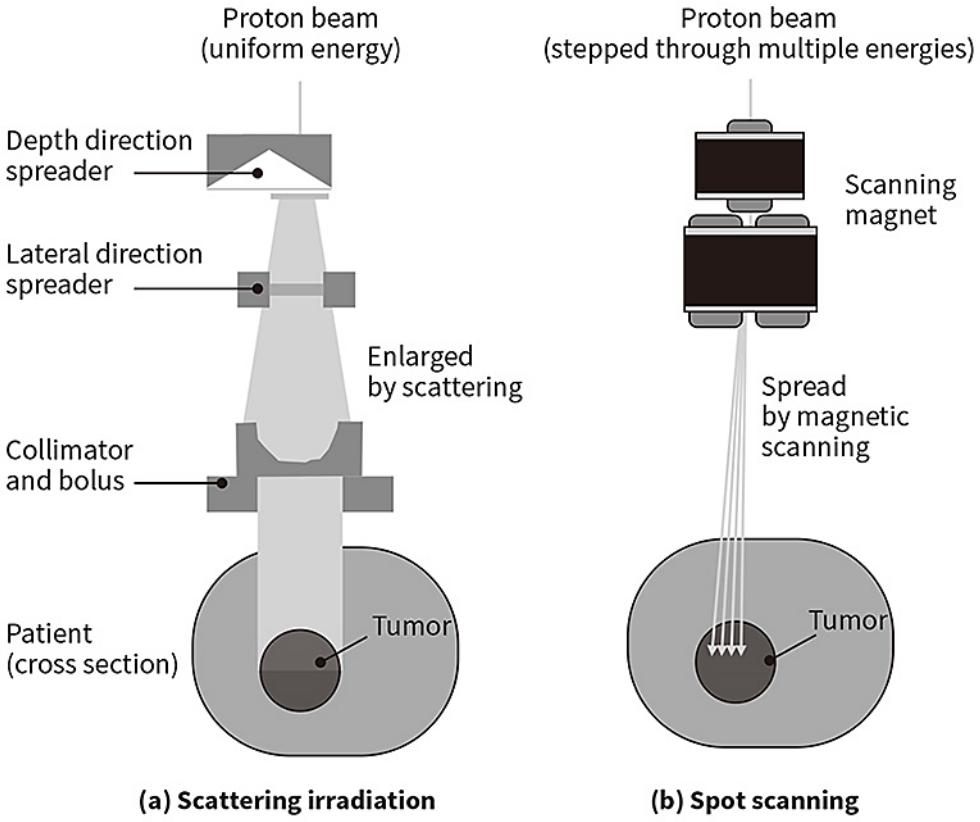

Fig.2.11. Schematic of passive scattering and (b) pencil beam scanning. This figure is adapted from [28].

At the South Florida Proton Therapy Institute, we use Pencil Beam Scanning technique. Therefore, we will focus only Pencil Beam Scanning (PBS).

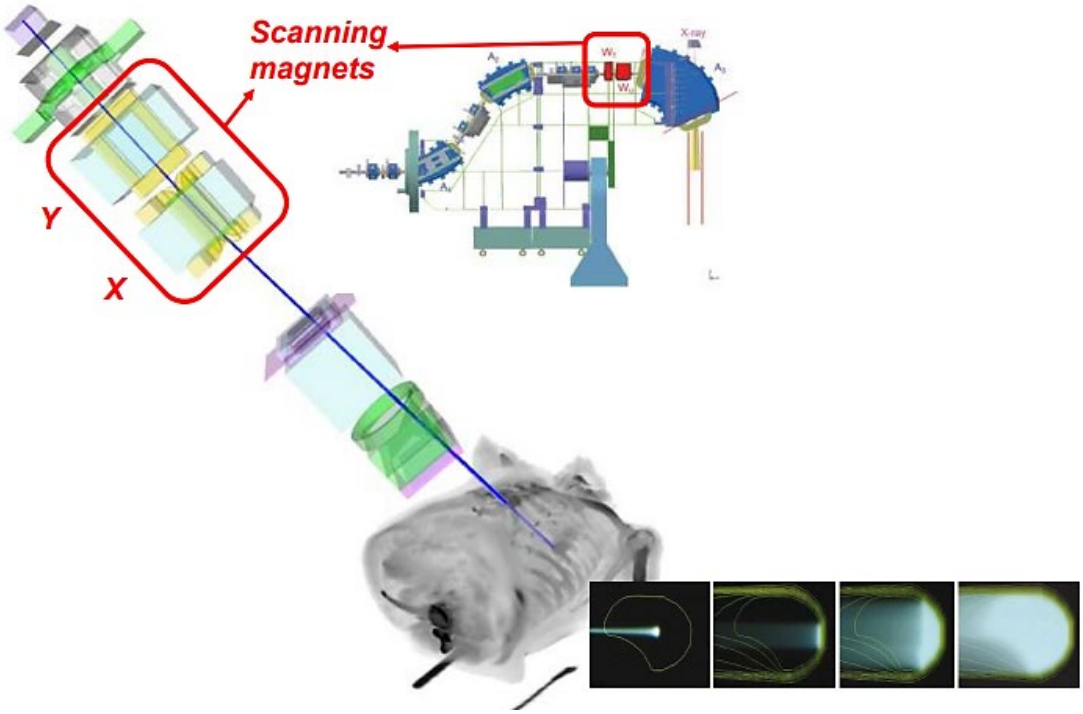

Fig.2.12. Pencil Beam Scanning Nozzle. This figure is adapted from [29].

The pencil beam scanning (PBS) technique consists of magnetically scanning pencil beams over a target volume, with the possibility of adjusting the position, energy, and fluence of the beams. [16] Because protons can be deflected magnetically, an alternative to the use of a broad beam is to generate a narrow mono-energetic "pencil" beam and to scan it magnetically across the target volume. This is a step&shoot process, where the spot at a static position is radiated with the dose and then the beam is switched off. After that the magnets are changed to target the next spot and so forth. The beam is scanned in a zigzag pattern in the x-y plane perpendicular to the beam direction. The depth

scan (z) is done by means of energy variation. The method requires neither a collimator nor a compensator. Radiation starts in the deepest levels with the highest energy in the x-y direction. In the next level the energy is reduced, and the layer is radiated. [30] Advantages of this technique are that it minimizes the interaction between the primary beam, and it minimizes the production of secondary particles. Further, it has the potential to treat complex tumor volumes with greater precision and improved normal tissue sparing. [31]

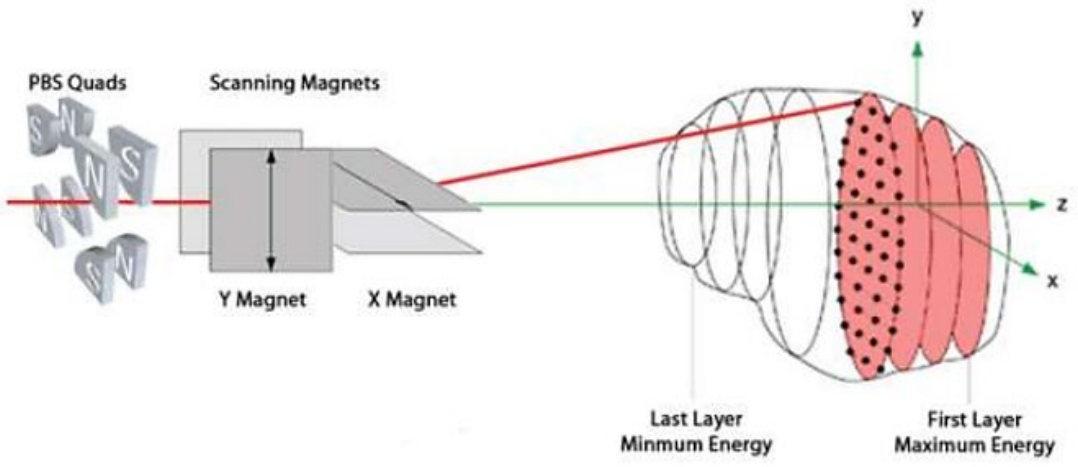

Fig.2.13. PBS spot map delivery. This figure is adapted from [31].

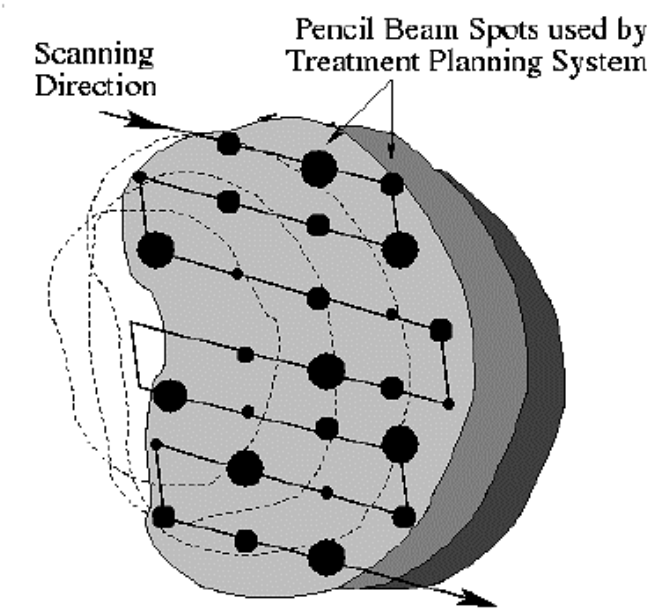

Fig.2.14. The principle of beam scanning: A narrow pencil beam is scanned across the target volume at various depths. The intensity can be varied from spot to spot, or continuously along the path. This figure is adapted from [32].

Pencil beam scanning has a nominal energy range from a 70 MeV (4.4 cm of water equivalent thickness – WET) to 220 MeV (30.2 cm WET). Using range shifter, the energy of 70 MeV it might be reduced if needed.

2.6.1 Treatment Planning System – TPS

At the South Florida Therapy Institute, commissioning of the Varian Compact Probeam machine was accomplished following the guidelines of the TRS-398 together with the methods used for commissioning of the Scripps proton therapy center (San Diego, California). Eclipse Treatment Planning System (Eclipse vs

15.6 TPS) supported by Varian was commissioned for delivery of PBS treatments. Some of the factors which affect treatment plan are spot profiles, integrated depth doses (IDDs), and absolute dose calibration.

- Spot profiles (σ) represents the lateral spread of the proton beam and can be differentiated into x and y-oriented profiles. They are defined as a single or double 2D Gaussian function. Smaller spot sizes give sharper dose gradients but are not recommended for large volume tumors.

$$\sigma = FWHM / 2.355 \quad (14)$$

- Integrated Depth Doses (IDD) is the total dose for a single spot over a very large plane normal to the beam direction. Before IDDs can be entered in the TPS they need to be corrected for the absolute dose and be multiplied by a value of 1.1 (RBE).
- Absolute dose is determined including different parameters like:
    - source-to-surface distance (SSD)
    - chamber type (chamber specific factor k_q is less stable at low values of residual range as the k_q curve becomes non-linear),
    - phantom material,
    - field size at phantom surface
    - measurement depth (z_{ref}) – if a mono-energetic beam is used then z_{ref} is specified in the middle of the SOBP or close to “plateau region”.

Equation used to calculate absorbed dose in water in proton beam of quality in the absence of chamber is:

$$D_{w,Q} = M_Q N_{D,w,Q_0} k_{Q,Q_0} \quad (15)$$

M_Q – is the dosimeter reading at a specific reference depth z_{ref} = 1.5cm. A correction of ion recombination, temperature, pressure, polarity, and electrometer calibration was performed prior to use.

N_{D,w,Q_0} – is the calibration factor for absorbed dose to water for a dosimeter at reference beam quality Q_0. The value for the absorbed dose to water term is found by calibration in a ^{60}Co beam.

k_{Q,Q_0} – is the correction for the difference in reference beam quality Q_o and user beam quality Q.

Residual range (R_{res}) defined as the practical range (R_p - depth at which the dose beyond the Bragg peak falls to 10% of its maximum) minus depth of measurement (z_{ref}) is called beam quality index according to TRS-398.

$$R_{res} = R_p - z_{ref} \quad (16)$$

Both, residual range (R_{res}) and practical range (R_p) are expressed in gcm^{-2}. [TRS-398]

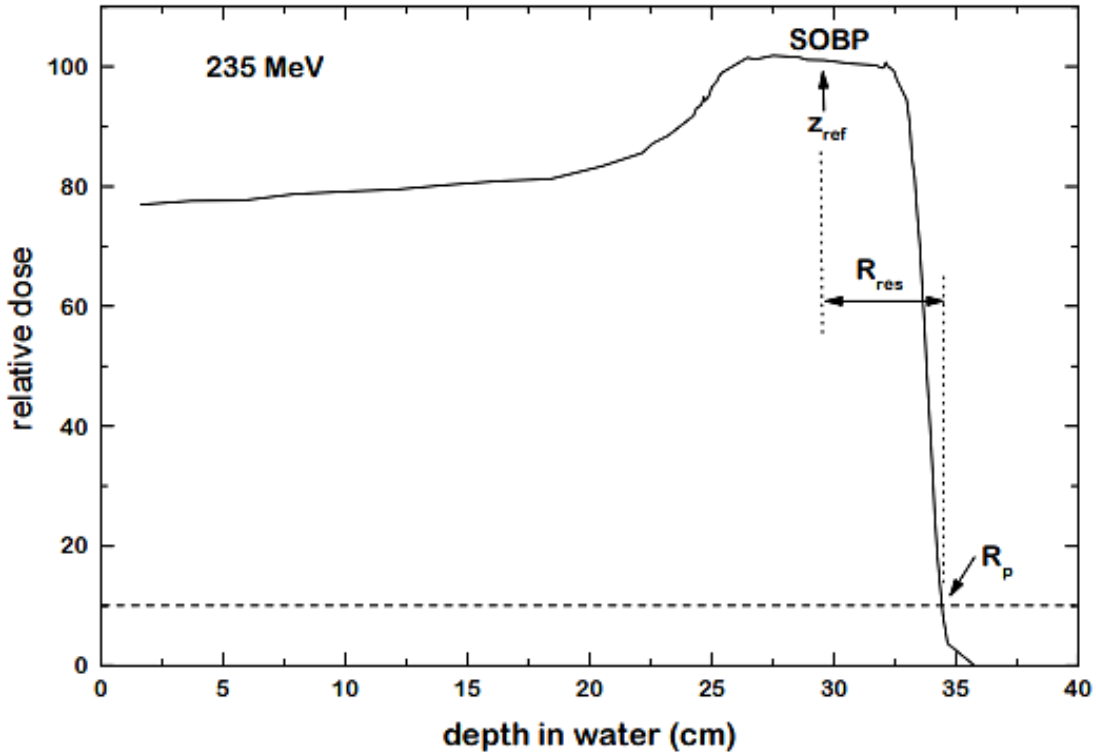

Fig.2.15. Percentage depth-dose distribution for a modulated proton beam. Indicated on the figure are the reference depth z_{ref} (middle of the SOBP), the residual range at z_{ref} used to specify the quality of the beam, Rres, and the practical range Rp. This figure is adapted from [TRS-398].

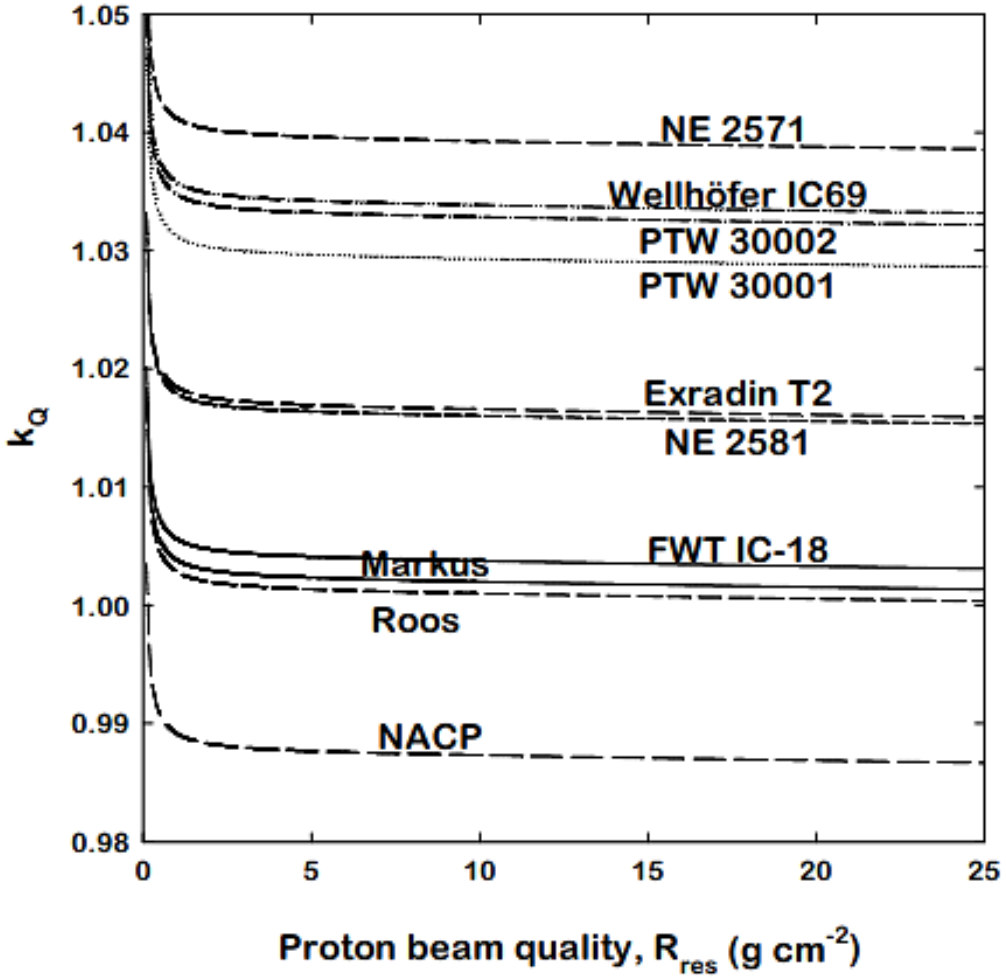

Fig. 2.16. Different values of k_q for different ionization chambers as a function of beam quality R_{res}. This figure is adapted from [TRS-398].

- Output factor: Knowing that the proton energy can be changed from 220 MeV to 70 MeV, energy dependence of the absolute dose calibration is described by output factor formula:

$$Output\ Factor = \frac{Dose(1.5cm)}{MU_{factor}} \quad (17)$$

MU_{factor} is the number of MU delivered per proton spot multiplied with the number of spots per mm^2.

$$MU_{factor} = \left(\frac{MU}{spot}\right) * \left(\frac{spot}{mm^2}\right) \quad (18)$$

At SFPTI based on these parameters: 32 MU per spot and 0.16 spots per square millimeter with 2.5 mm spot spacing, MU factor was 5.12. Absolute and relative output factors for energies between 70 MeV and 220 MeV were calculated in 5 MeV steps.

Table 2.2. Reference conditions for the determination of absorbed dose in proton beams. This table is adapted from [TRS-398].

Influence quantity	Reference value or reference characteristics
Phantom material	water
Chamber type	for $R_{res} \geq 0.5$ g cm^{-2}, cylindrical and plane-parallel. for $R_{res} < 0.5$ g cm^{-2}, plane-parallel.
Measurement depth z_{ref}	middle of the SOBP [a]
Reference point of chamber	for plane-parallel chambers, on the inner surface of the window at its centre. For cylindrical chambers, on the central axis at the centre of the cavity volume
Position of reference point of chamber	for plane-parallel and cylindrical chambers, at the measurement depth z_{ref}.
SSD	clinical treatment distance
Field size at the phantom surface	10 cm x 10 cm, or that used for normalization of the output factors whichever is larger. For small field applications (i.e. eye treatments), 10 cm x 10 cm or the largest field clinically available

[a] The reference depth can be chosen in the "plateau region", at a depth of 3 g cm^{-2}, for clinical applications with a mono-energetic proton beam (e.g. for plateau irradiations).

Table 2.3. Reference conditions for the determination of absorbed dose in proton beam quality. (R_{res}). This table is adapted from [TRS – 398].

Influence quantity	Reference value or reference characteristics
Phantom material	water
Chamber type	cylindrical and plane-parallel
Reference point of chamber	for plane-parallel chambers, on the inner surface of the window at its centre. For cylindrical chambers, on the central axis at the centre of the cavity volume
Position of reference point of chamber	for plane-parallel and cylindrical chambers, at the point of interest
SSD	clinical treatment distance
Field size at the phantom surface	10 cm x 10 cm For small field applications (i.e. eye treatments), 10 cm x 10 cm or the largest field clinically available

2.6.2 The algorithm of Pencil Beam Scanning in Proton Therapy

Treatment planning systems in proton beam therapy use different algorithms to calculate the delivered dose. Currently there are two classes of algorithms in PBS: pencil beam (PB) and Monte-Carlo (MC) algorithm.

- PB algorithms are analytical in nature and for the same set of input parameters it has been shown that we have a constant dose distribution. Calculation algorithms on the MC use random sampling of interaction cross-sections to simulate individual particles trajectories. Dose calculation in PB algorithm is the convolution of proton fluence, ø, and the elemental pencil beam dose distribution called dose kernel K. [33]

$$Dose = \emptyset \otimes K \tag{19}$$

Clinically, discrete grids are used to calculate the dose by a summation in X, Y and Z directions:

$$Dose\ (X, Y, Z) = \Sigma Xi\ \Sigma Yi\ \emptyset\ (X - Xi, Y - Yi, Z)\ K\ (X - Xi, Y - Yi, Z) \tag{20}$$

$$K(x, y, z) = N_{p^+} + ID\ \frac{1}{2\pi\sigma_x\sigma_y}\ exp\left[-\frac{(x_0-x)^2}{2\sigma_x^2}\right] exp\left[-\frac{(y_0-y)^2}{(y_0-2\sigma_y^2)}\right] \tag{21}$$

N_{p^+} – is the number of protons in a beam spot,

$\sigma_x\sigma_y$ – the standard deviations of spot intensity.

- **Monte Carlo Algorithm (MC)**

Radiation transport equation for MC algorithm is solved by using random numbers and probability density distributions to represent the underlying physical interactions. This method it tracks individual particles energies, and after the deposition of these energies in respective voxel, the dose distribution is formed by summing all of them. To compute the dose from a spot in a PBS, MC calculation it starts after randomly picking primary protons and transporting them through modifying beam devices, air gaps and then into the patients. [34, 35] At the South Florida Proton Therapy Institute the algorithm used to calculate the dose distribution in Eclipse 15.6 planning system is MC AcurosPT. Radiation transport in AcurosPT is split in four phases: (I) interaction with atomic electrons (slowing down), (II) elastic nuclear Coulomb scattering, (III) elastic strong force scattering, and (IV) non elastic nuclear interactions. By using a phase space approach, the model implemented in AcurosPT is the double Gaussian fluence. [36] Halo effect that is created upstream from the treatment volume, and in a range shifter this is not modeled in Monte Carlo algorithm, and it can lead to dose discrepancies. Range shifters for shallow treatment are expected to exacerbate the halo effect. [6] Usage of RS makes the spot sizes to increase, especially for low proton energies. This is a result of scattering of protons from the RS and the large air gap between the RS and isocenter. The large-angle multiple Coulomb scattering and nuclear interactions are the factors that the RS creates low-signal tails in the beam profile due to large-angle multiple Coulomb scattering and nuclear interactions. [37] In our study, we include measurement of field size

factors with one range shifter of 5.68 cm, so we can calculate these discrepancies over the calculations of TPS.

Chapter 3: Methods and Material

3.1 *Treatment planning system*

All treatment plans for this study were generated using the Eclipse Treatment Planning System (vs15.6 TPS). We have created dose cubic with different field sizes (X, Y) 2cm x 2cm, 3cm x 3cm, 5cm x 5cm, 10cm x 10cm, 20cm x 20cm with a fixed depth coverage (Z) of 6cm, where the center of the dose cloud (ISO) depends on the energy ranges. Clearly, the center of dose cloud in our plan or comparison plane is always at ProBeam ISO center. Different SAD plans at ISO depth 5cm 15cm and 25cm for different field sizes have been measured. After that we have exported coronal planar dose map at ISO to compare the measurements at ISO. Such comparison has been repeated with plans having the 5.68cm range shift only.

Some of the parameters used in planning of those fields are shown in the table below.

Table 3.1. Treatment planning parameters.

Dose per fraction [cGy]	300
Number of fractions	1
Calculation resolution in cm	0.1
Spot spacing in scanning direction in cm	0.5
Spacing between scanning layers in cm	0.5

3.2 Phantom and detector

Our measurements were conducted in a RW3 Slab Phantom (PTW, Freiburg,Germany). The RW3 phantom is water-equivalent material (Goettingen White Water) in the energy ranges from ^{60}Co to 25 MV photons and from 4 MeV to 25 MeV electrons. Each plate is precisely machined for a thickness tolerance of only ± 0.1 mm. [38] This phantom was placed on the treatment table where it was irradiated from the top at a gantry angle of 0°.

We have used Octavius Detector 1500XDR (PTW) for measuring the absolute doses of the specific fields. The softer used for comparing these doses was PTW-VeriSoft 7.2.

For all the measurement we have used constant parameters to compare the RT plan with the measured ones. The gamma index is used to determine the outcome (pass-fail). Gamma 2D parameters used are: 2.0 mm distance – to – agreement, 2.0% dose difference with reference to local dose, we used increased tolerance of 5.0 % dose diff. for values below 0.2 Gy (or AU).

Table 3.2. Octavius 1500XDR parameters. This table is adapted from [39].

Detector type	Plane-parallel vented ionization chamber
Number of detectors	1405
Detector size:	4.4 mm x 4.4 mm x 3 mm (0.06 cm^3)
Detector spacing:	7.1 mm center-to-center
Max. field size:	27 x 27 cm^2
Max. measurement points:	2916 (four merged measurements)
Reproducibility:	≤ ± 0.5%
Dead time:	zero
Repetition rate:	100 ms
Measured quantities:	absorbed dose to water (Gy), absorbed dose rate to water (Gy/min)
Resolution:	Dose: 0.1 mGy, Dose rate: 0.1 mGy/min
Measurement range:	0.25 ... 800 Gy/min
Reference point:	7.5 mm below the surface of the array
Housing material:	PS, GRP (frame)
Dimensions:	30 cm x 46.7 cm x 2.2 cm (W x D x H)
Weight:	6 kg
Power supply:	(100 ... 240) VAC; (50 ... 60) Hz
PC connection:	Ethernet

Corrections for temperature (20.5°C) and pressure (115.08hPa) has been conducted prior to each measurement with a Precision Digital Barometer and Thermometer Model DBT-100, which has an accuracy of ±0.5 mbar, includes non-linearity, hysteresis, and repeatability ±0.2º C, includes non-linearity.

Chapter 4: Results and Discussion

In planning system, in PCS algorithm we use single gaussian but in reality, this portion is slightly higher. Double gaussian can be used in PCS and in water measurement has been shown to be very accurate nonetheless, PCS algorithm in certain situations misses a lot of scatters in patient, where we may have issues especially for tissue heterogeneities. However, AcuroPT can deal with the tissue heterogeneities. We assume that as field size increases, and the use of range shifter and air gap will exacerbate the discrepancies between RT plan and measured dose. Now the question is which one of the algorithms will give more precise results.

In our study we have been focused on comparison of PCS vs. Measured dose, AcurosPT vs. Measured dose, and comparison between PCS vs. AcurosPT.

4.1 ISO at 5cm

From this study we found that the clinical TPS – AcurosPT it overestimates the output at 5cm ISO by as much as 5.62% in 2cm field with a 5cm air gap. Whereas, for the same field PCS it underestimates the output by 5.16%.

In 2cm field with 5cm air gap and 5.68cm range shifter AcurosPt delivers 3.67% less dose than PCS, whereas in bigger fields, 10cm and 20cm field PCS delivers

less dose than AcurosPT up to 7.73% and 10.86% respectively.

In the next tables below PCS is referenced as “P” and AcurosPT as “A”.

Table 4.1. TPS and dose output at the isocenter of 5cm WET.

SOBP 5cm WET		TPS (Gy)	Measurement (Gy)
2x2x6, RS 5cm, and 5cm Air gap	*P*	2.965	2.947
	A	2.855	2.945
3x3x6, RS 5cm, and 5cm Air gap	*P*	3.021	3.043
	A	3.002	3.032
5x5x6, RS 5cm, and 5cm Air gap	*P*	3.031	3.092
	A	3.099	3.087
10x10x6, RS 5cm, and 5cm Air gap	*P*	3.011	3.160
	A	3.246	3.151
20x20x6, RS 5cm, and 5cm Air gap	*P*	3.026	3.182
	A	3.363	3.174

Table 4.2. Normalized dose values for comparisons of PCS and AcurosPT against the measured for SOBP at 5cm WET with 5cm air gap and 5cm RS.

SOBP 5cm WET	*PCS/ Measured*	*(±) % Error*	*AcurosPT/ Measured*	*(±) % Error*	*Measured*
2x2x6	100.61	0.61	96.94	3.05	100
3x3x6	99.27	-0.72	99.01	-0.99	100
5x5x6	98.02	-1.97	100.38	0.38	100
10x10x6	95.28	4.71	103.01	3.01	100
20x20x6	95.09	4.90	105.95	5.95	100

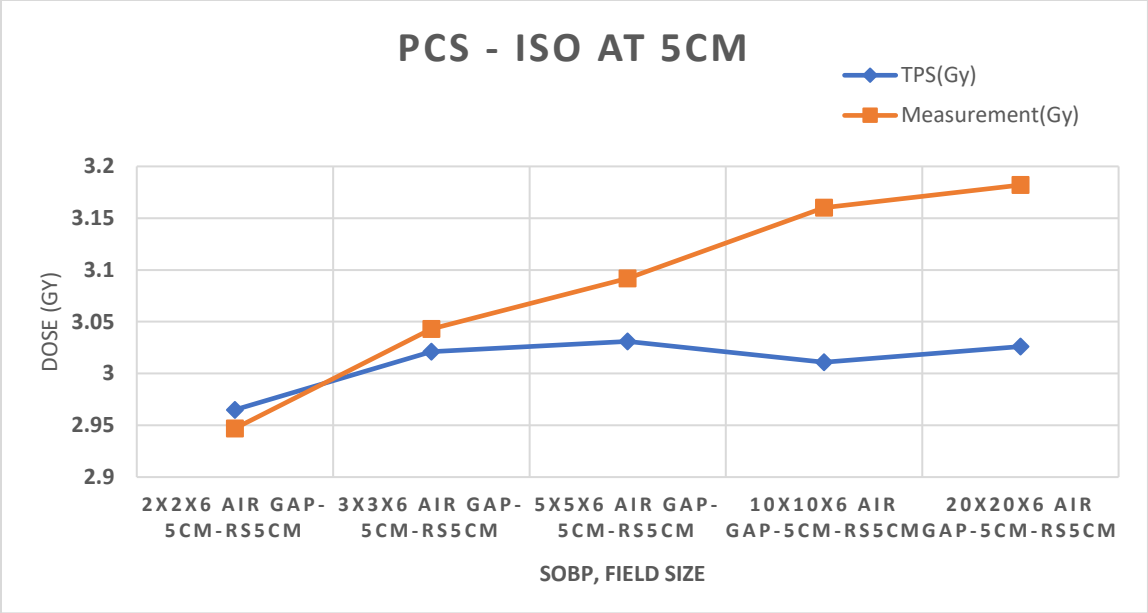

Fig.4.1. Dose comparison in PCS algorithm with an isocenter at 5 cm WET.

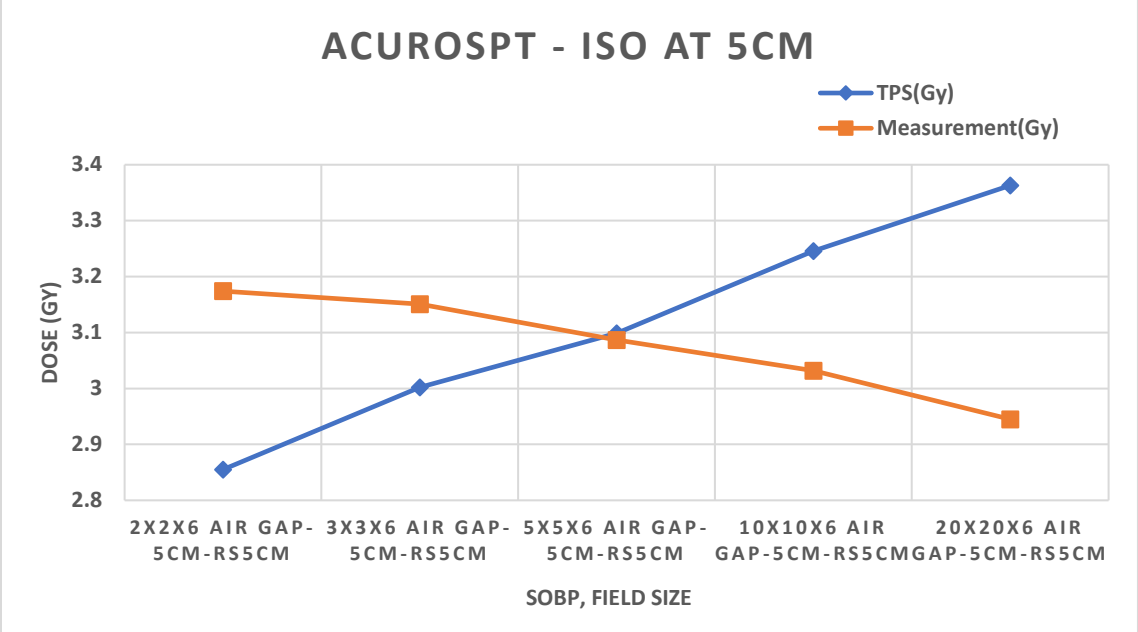

Fig.4.2. Dose comparison in AcurosPT algorithm with an isocenter at 5cm WET.

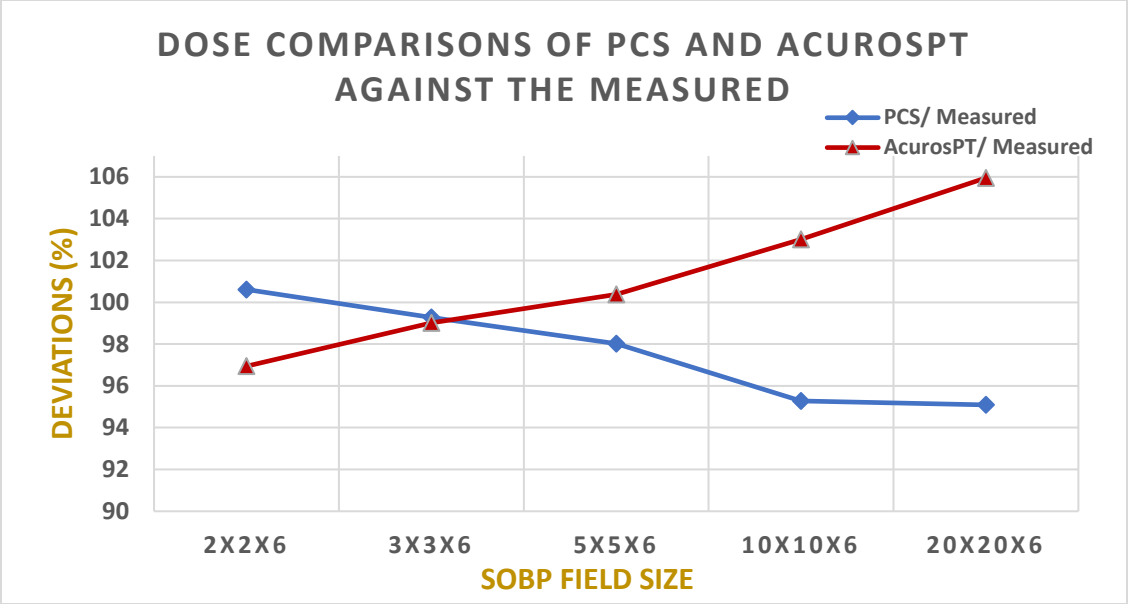

Fig.4.3. Comparison of Measured doses against those in of P and A plans for ISO at 5cm WET, RS 5cm, and 5cm Air gap.

4.2 ISO at 10cm

For SOBP at 10cm ISO we have studied all the field sizes in open conditions and also each field has been studied with 5cm, 15cm, and 25cm air gap with 5.68cm range shifter.

From the table 4.3, 4.4 and figures 4.4 to 4.18 we can clearly see that partial involvement of halo in TPS has the biggest impact in the small fields, especially in 2cm field with 25cm airgap and the involvement of the range shifter. AcurosPT it underestimates the dose by as much as 8.14%. For field sizes between 3cm and 10cm the difference is relatively constant in the range of +2.75% for TPS (AcurosPT) in 3cm, to -3.62% for TPS (PCS) in 10cm with 15cm air gap and 5.68 cm range shifter. In bigger fields the difference goes up to 6.9% for 20cm field with air gap of 15cm and range shifter (AcurosPT).

From our data we find out that for small fields like 2cm AcurosPT in shallower targets (15cm air gap) delivers 8.07% less dose than PCS and for deeper targets the deviation is smaller, only 0.44%. For bigger fields, AcurosPT in shallower depth delivers up to 12.94% more dose than PCS, and in deeper depth it delivers 8.74% more dose than PCS.

Table 4.3. TPS and dose output at the isocenter of 5cm WET.

ISO at 10cm WET		TPS (Gy)	Measurement (Gy)
2x2x6	*P*	3.003	2.964
	A	2.985	2.959
2x2x6, RS 5cm, and 5cm Air gap	*P*	2.970	2.952
	A	2.867	2.951
2x2x6, RS 5cm, and 15cm Air gap	*P*	2.793	2.775
	A	2.572	2.776
2x2x6, RS 5cm, and 25cm Air gap	*P*	2.798	2.817
	A	2.603	2.815
3x3x6	*P*	3.056	3.019
	A	3.096	3.011
3x3x6, RS 5cm, and 5cm Air gap	*P*	3.039	3.055
	A	3.065	3.066
3x3x6, RS 5cm, and 15cm Air gap	*P*	3.122	3.148
	A	3.124	3.157
3x3x6, RS 5cm, and 25cm Air gap	*P*	3.105	3.168
	A	3.124	3.178
5x5x6	*P*	3.035	3.044
	A	3.124	3.042
5x5x6, RS 5cm, and 5cm Air gap	*P*	3.040	3.103
	A	3.142	3.114
5x5x6, RS 5cm, and 15cm Air gap	*P*	3.091	3.163
	A	3.159	3.167
5x5x6, RS 5cm, and 25cm Air gap	*P*	3.394	3.478
	A	3.453	3.512
10x10x6	*P*	3.006	3.062
	A	3.150	3.057
10x10x6, RS 5cm, and 5cm Air gap	*P*	3.046	3.142
	A	3.253	3.151
10x10x6, RS 5cm, and 15cm Air gap	*P*	3.035	3.145
	A	3.223	3.161
10x10x6, RS 5cm, and 25cm Air gap	*P*	3.126	3.222
	A	3.275	3.239
20x20x6	*P*	3.036	3.10
	A	3.308	3.101
20x20x6, RS 5cm, and 5cm Air gap	*P*	3.044	3.176
	A	3.395	3.177
20x20x6, RS 5cm, and 15cm Air gap	*P*	3.020	3.197
	A	3.436	3.199
20x20x6, RS 5cm, and 25cm Air gap	*P*	3.026	3.229
	A	3.428	3.235

Table 4.4. Normalized dose values for comparisons of PCS and AcurosPT against the measured for SOBP at 10cm WET.

SOBP 10cm WET	PCS/ Measured	(±) % Error	AcurosPT/ Measured	(±) % Error	Measured
2x2x6	101.31	1.31	100.87	0.87	100
2x2x6, RS 5cm, and 5cm Air gap	100.60	0.60	97.15	-2.84	100
2x2x6, RS 5cm, and 15cm Air gap	100.64	0.64	92.57	-7.42	100
2x2x6, RS 5cm, and 25cm Air gap	99.32	-0.67	92.46	-7.53	100
3x3x6	101.22	1.22	102.82	2.82	100
3x3x6, RS 5cm, and 5cm Air gap	99.47	-0.53	99.96	-0.04	100
3x3x6, RS 5cm, and 15cm Air gap	98.85	-1.15	98.95	-1.05	100
3x3x6, RS 5cm, and 25cm Air gap	98.01	-1.99	98.64	-1.36	100
5x5x6	99.70	-0.30	102.69	2.69	100
5x5x6, RS 5cm, and 5cm Air gap	97.96	-2.04	100.89	0.89	100
5x5x6, RS 5cm, and 15cm Air gap	97.72	-2.28	99.75	0.25	100
5x5x6, RS 5cm, and 25cm Air gap	97.58	-2.42	99.28	-0.72	100
10x10x6	98.17	-1.83	103.04	3.04	100
10x10x6, RS 5cm, and 5cm Air gap	96.94	-3.06	103.23	3.23	100
10x10x6, RS 5cm, and 15cm Air gap	96.5	-3.5	101.96	1.96	100
10x10x6, RS 5cm, and 25cm Air gap	97.02	2.98	101.11	1.11	100
20x20x6	97.93	-2.07	106.67	6.67	100
20x20x6, RS 5cm, and 5cm Air gap	95.84	-4.16	106.86	6.86	100
20x20x6, RS 5cm, and 15cm Air gap	94.46	-5.54	107.4	7.40	100
20x20x6, RS 5cm, and 25cm Air gap	93.71	-6.29	105.96	5.96	100

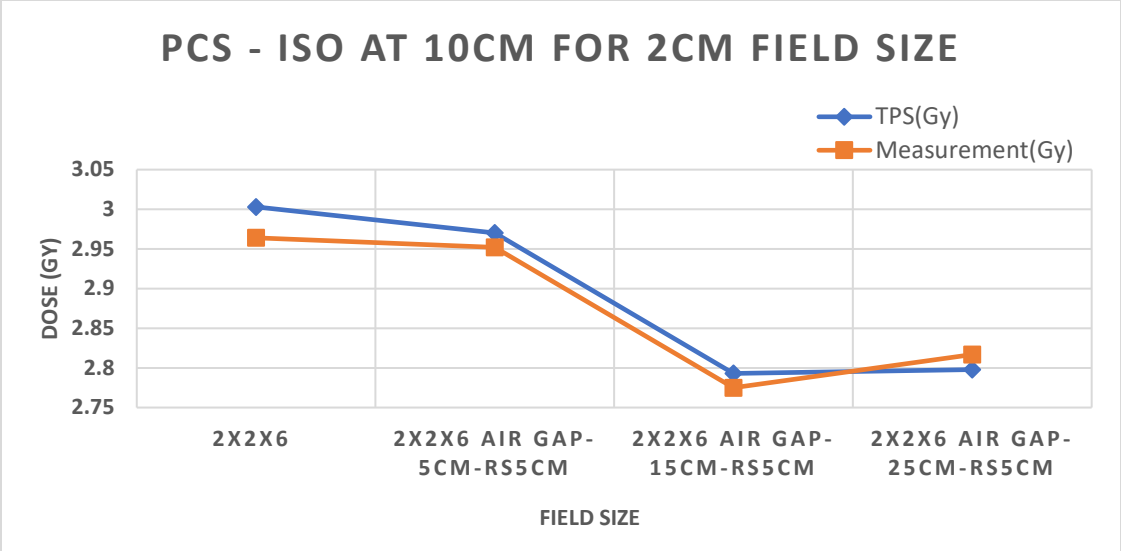

Fig.4.4. Dose comparison in PCS algorithm with an isocenter at 10cm WET, for 2cm field and with 5cm, 15cm, and 25 cm air gaps, including 5.68cm range shifter.

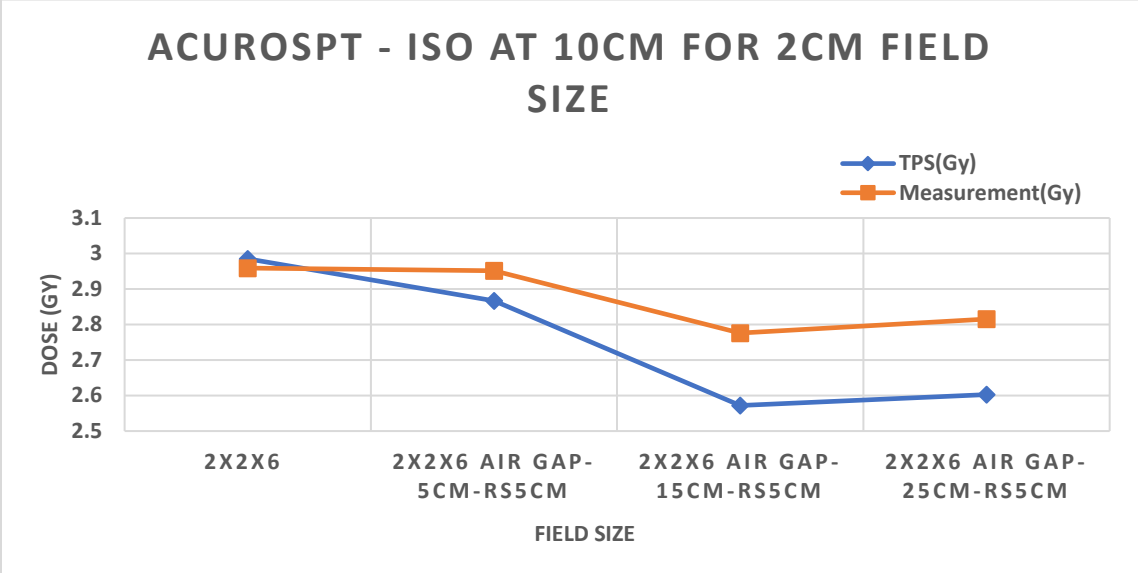

Fig.4.5. Dose comparison in AcurosPT algorithm with an isocenter at 10cm WET, for 2cm field and with 5cm, 15cm, and 25 cm air gaps, including 5.68cm range shifter.

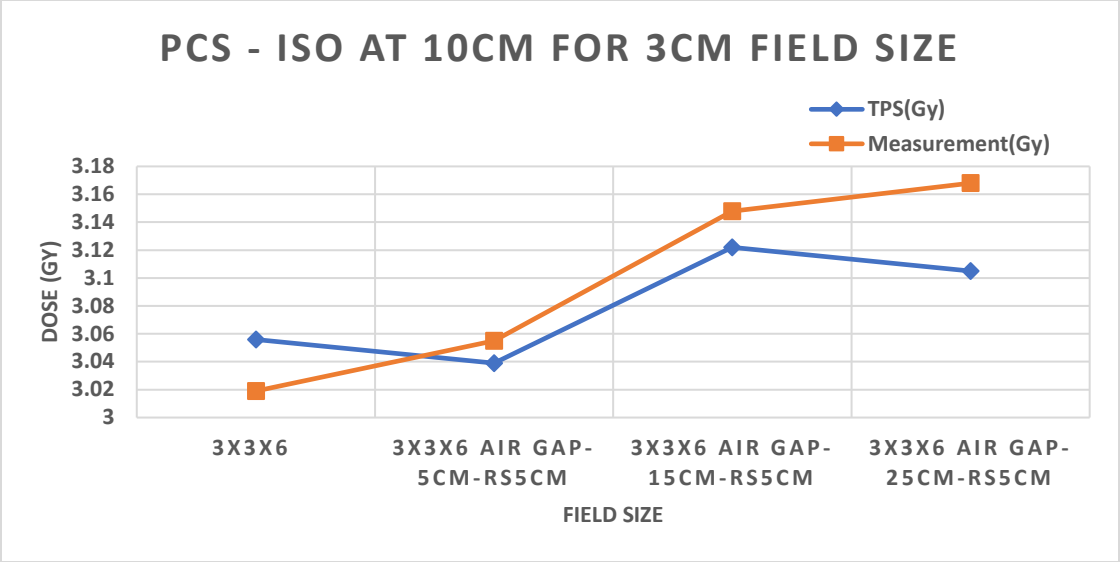

Fig.4.6. Dose comparison in PCS algorithm with an isocenter at 10cm WET, for 3cm field and with 5cm, 15cm, and 25 cm air gaps, including 5.68cm range shifter.

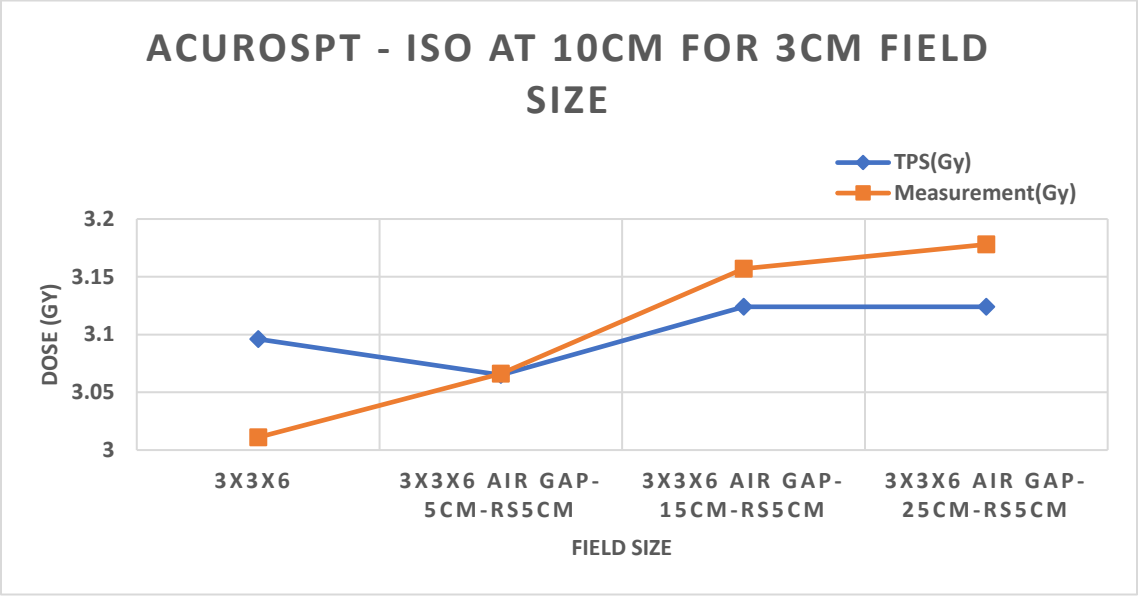

Fig.4.7. Dose comparison in AcurosPT algorithm with an isocenter at 10cm WET, for 3cm field and with 5cm, 15cm, and 25 cm air gaps, including 5.68cm range shifter.

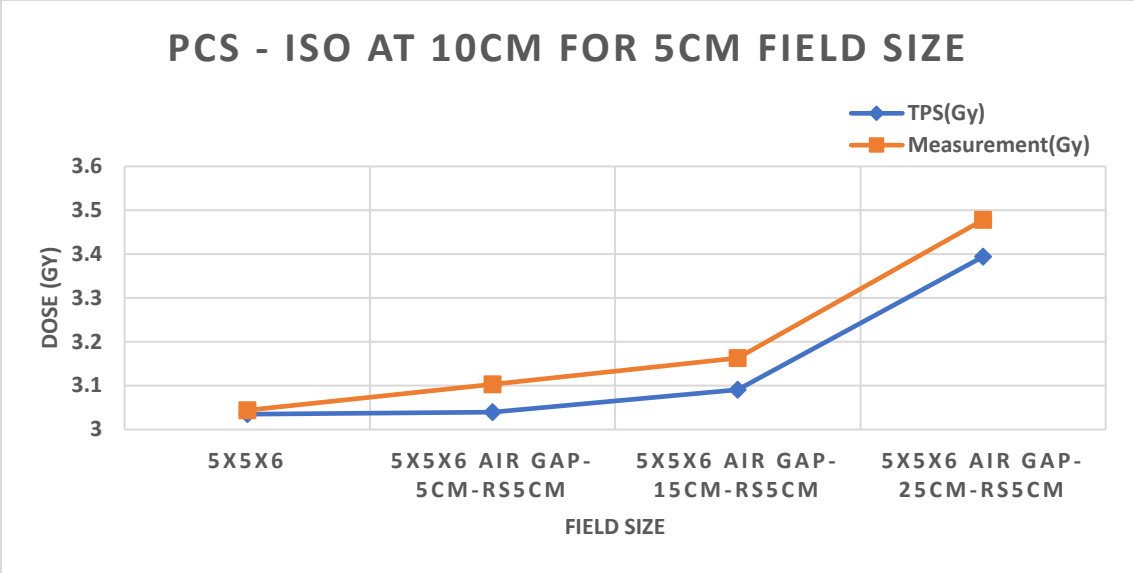

Fig.4.8. Dose comparison in PCS algorithm with an isocenter at 10cm WET, for 5cm field and with 5cm, 15cm, and 25 cm air gaps, including 5.68cm range shifter.

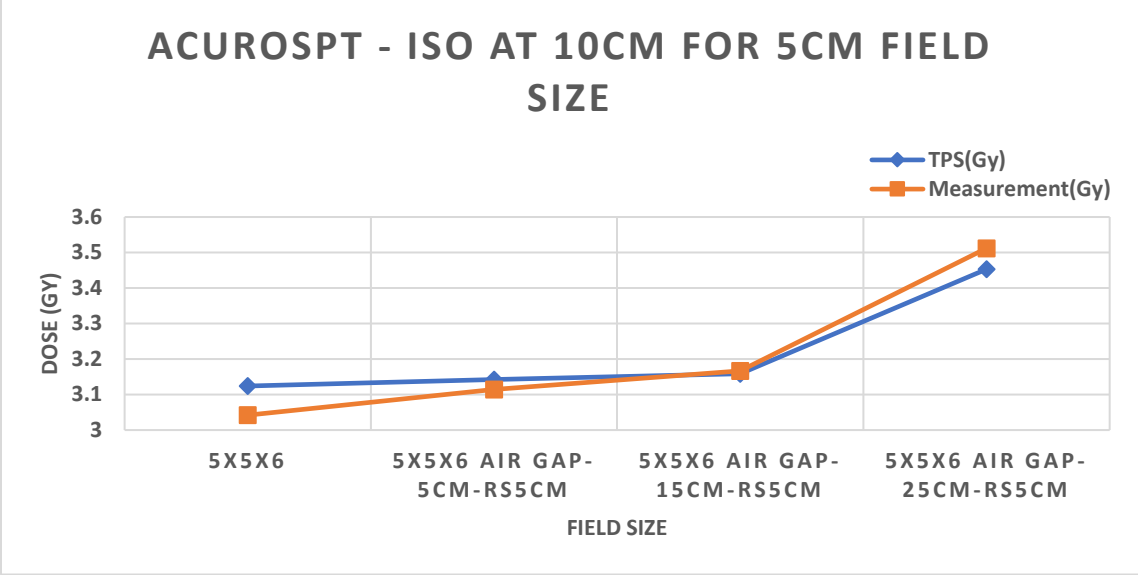

Fig.4.9. Dose comparison in AcurosPT algorithm with an isocenter at 10cm WET, for 5cm field and with 5cm, 15cm, and 25 cm air gaps, including 5.68cm range shifter.

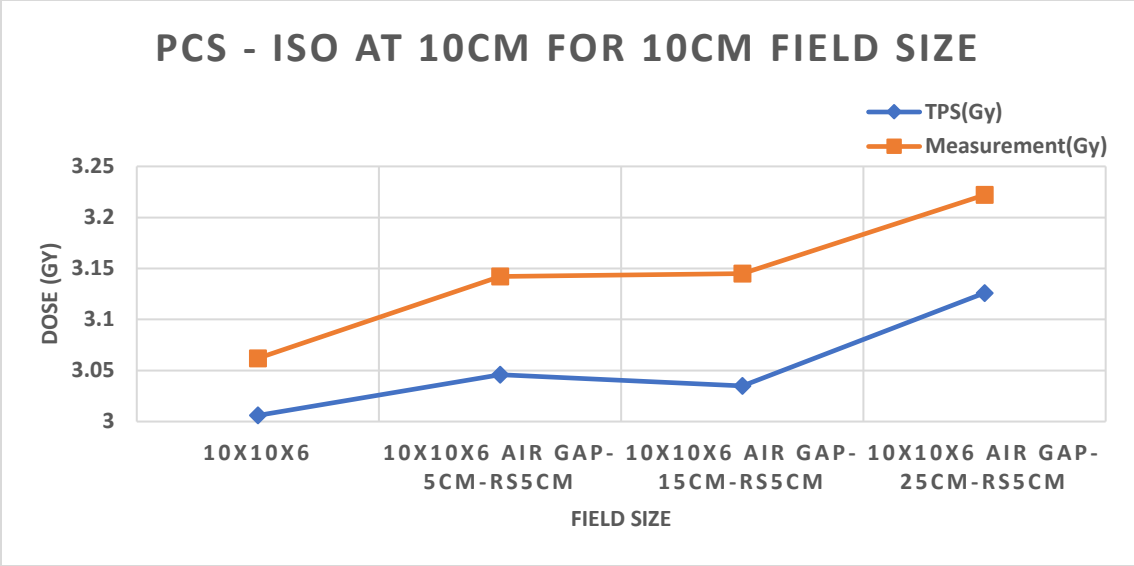

Fig.4.10. Dose comparison in PCS algorithm with an isocenter at 10cm WET, for 10cm field and with 5cm, 15cm, and 25 cm air gaps, including 5.68cm range shifter.

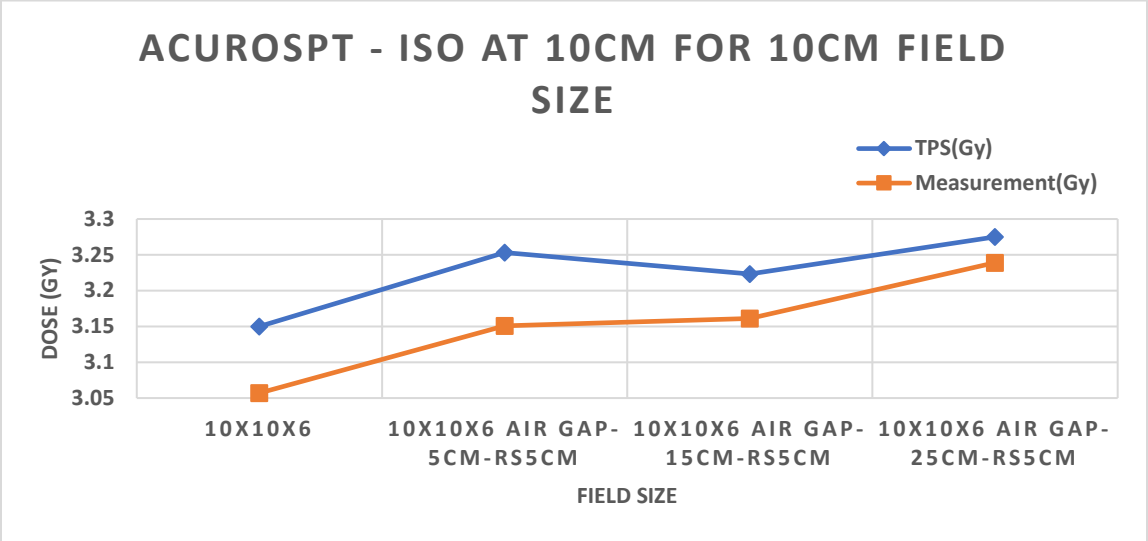

Fig.4.11. Dose comparison in AcurosPT algorithm with an isocenter at 10cm WET, for 10cm field and with 5cm, 15cm, and 25 cm with air gaps, including 5.68cm range shifter.

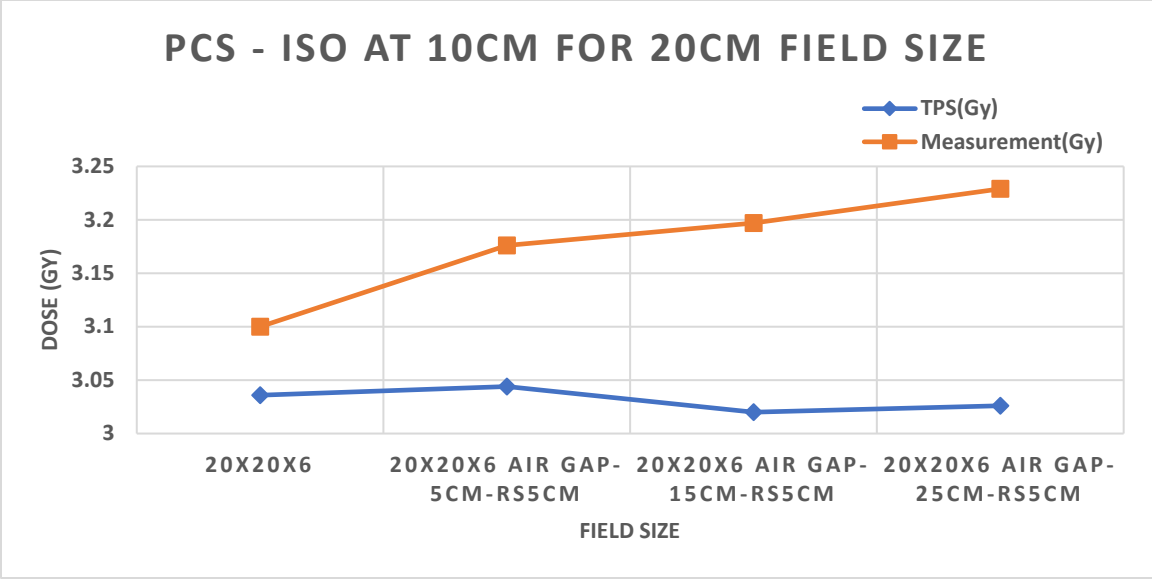

Fig.4.12. Dose comparison in PCS algorithm with an isocenter at 10cm WET, for 20cm field and with 5cm, 15cm, and 25 cm air gaps, including 5.68cm range shifter.

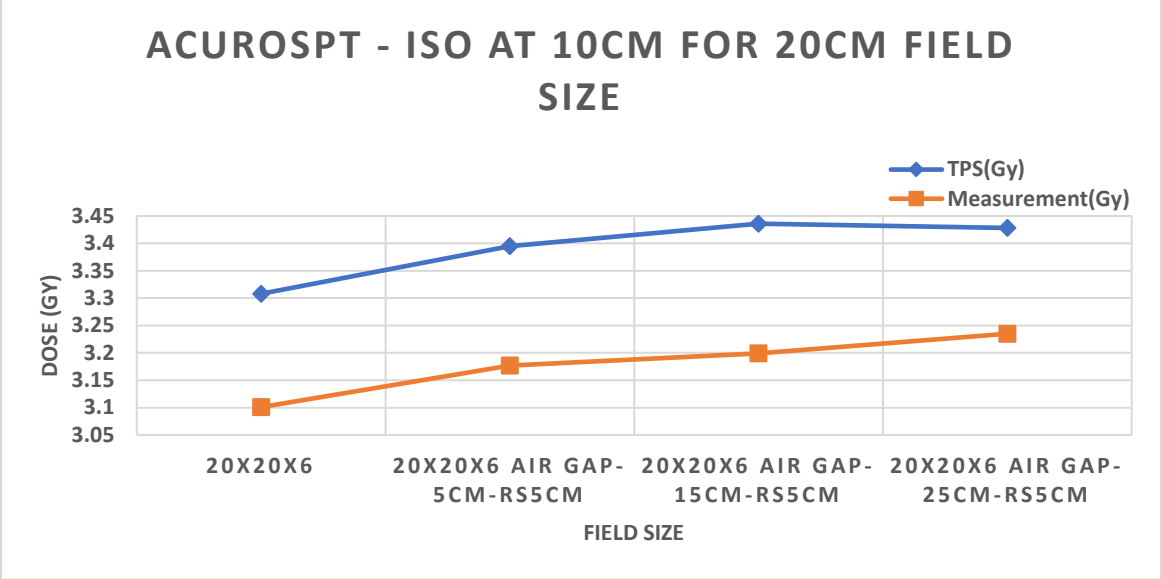

Fig.4.13. Dose comparison in AcurosPT algorithm with an isocenter at 10 cm WET, for 20cm field and with 5cm, 15cm, and 25 cm air gaps, including 5.68cm range shifter.

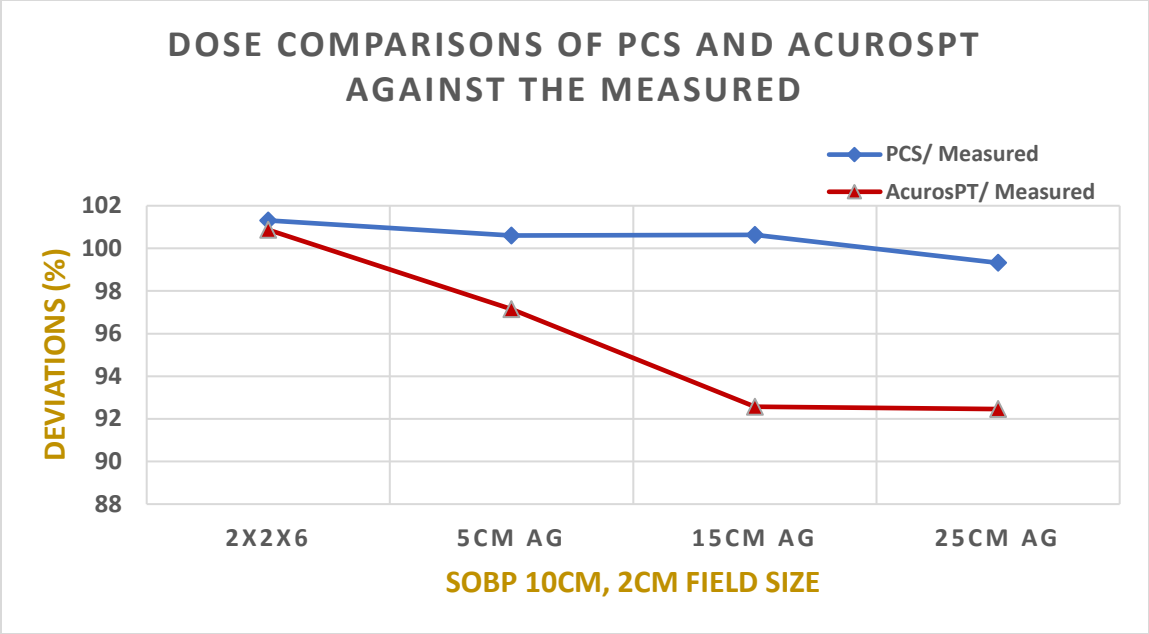

Fig.4.14. Comparison of measured doses against those in of P and A plans for a 2cm field at ISO 10cm WET, RS 5cm, and 5cm Air gap.

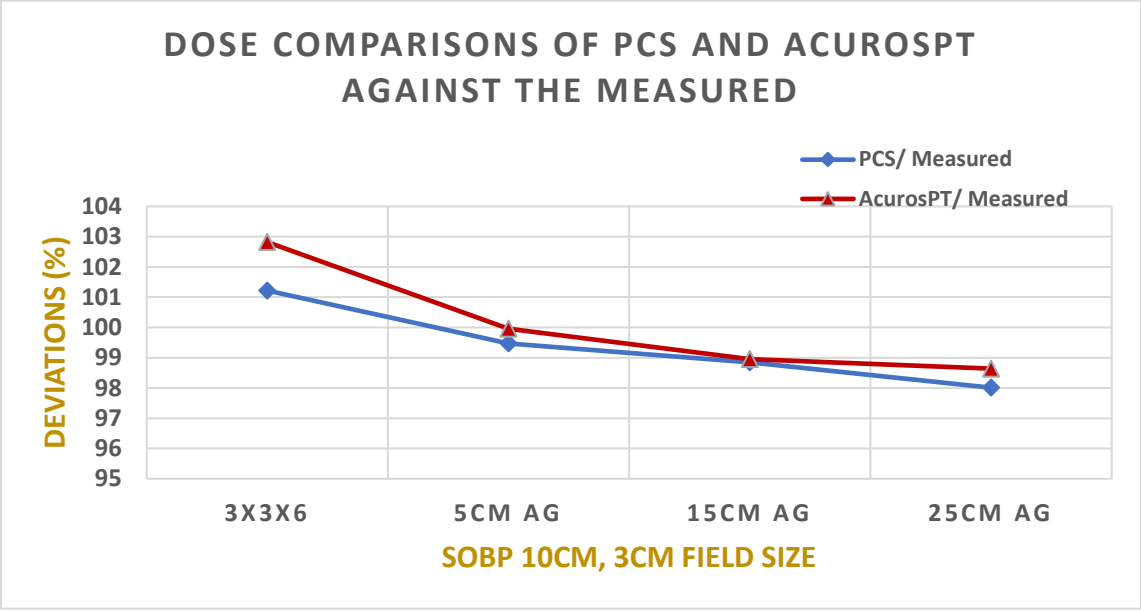

Fig.4.15. Comparison of measured doses against those in of P and A plans for a 3cm field at ISO 10cm WET, RS 5cm, and 5cm Air gap.

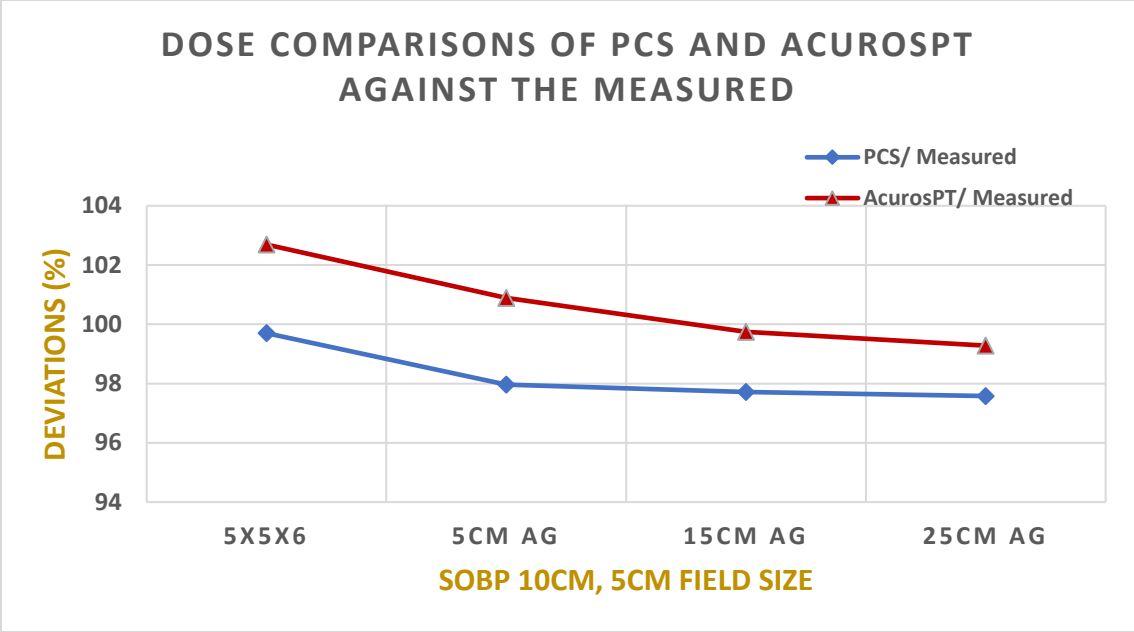

Fig.4.16. Comparison of measured doses against those in of P and A plans for a 5cm field at ISO 10cm WET, RS 5cm, and 5cm Air gap.

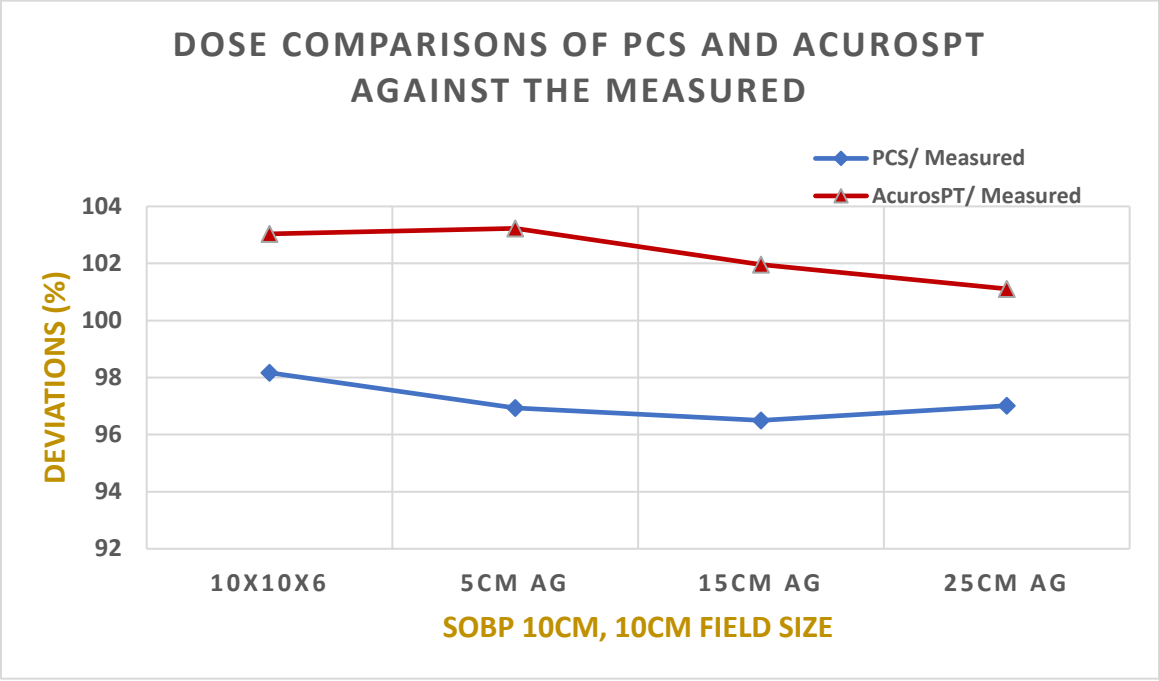

Fig.4.17. Comparison of measured doses against those in of P and A plans for a 10cm field at ISO 10cm WET, RS 5cm, and 5cm Air gap.

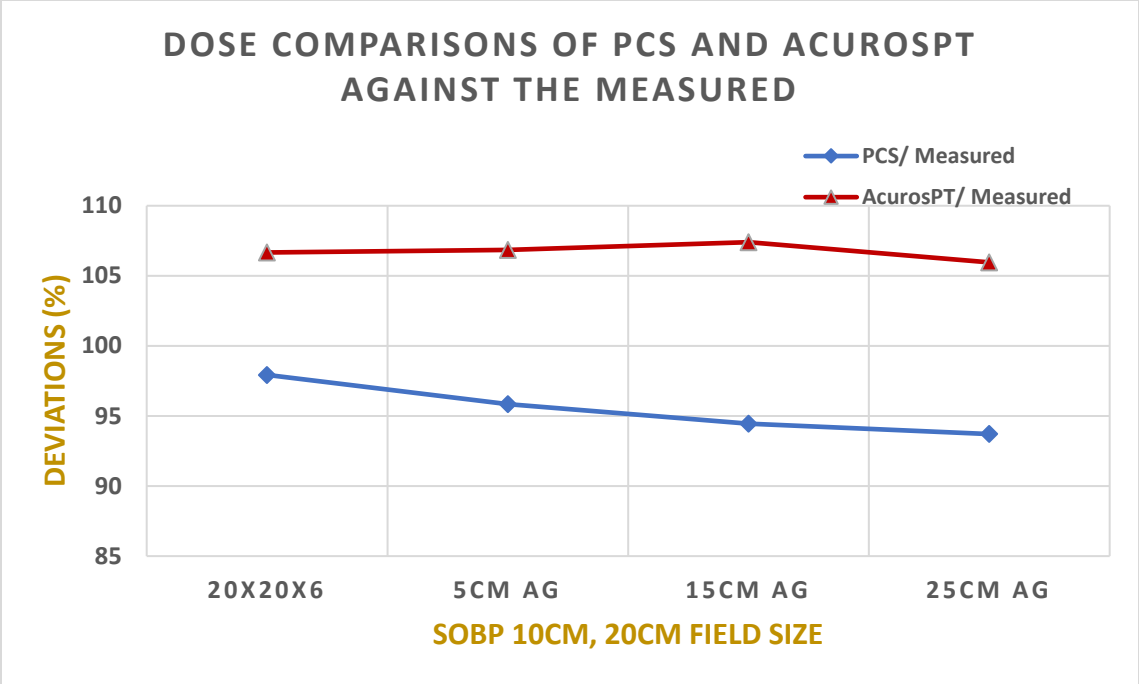

Fig.4.18. Comparison of measured doses against those in of P and A plans for a 20cm field at ISO 10cm WET, RS 5cm, and 5cm Air gap.

4.3 ISO at 20cm

At 20 cm isocenter discrepancies between TPS and measured data for both algorithms is small. We have -1.33% at TPS dose for AcurosPT algorithm in 2cm and -3.23% at TPS dose for PCS algorithm in 10cm. We noticed a bigger difference for larger fields like 20cm. This difference is +6.24% TPS (AcurosPT).

Table 4.5. TPS and dose output at the isocenter of 20cm WET.

ISO at 20cm WET		TPS (Gy)	Measurement (Gy)
2x2x6	P	2.998	2.910
	A	2.932	2.971
3x3x6	P	3.021	3.043
	A	3.892	3.938
5x5x6	P	3.050	3.083
	A	3.144	3.111
10x10x6	P	3.933	4.060
	A	4.193	4.081
20x20x6	P	3.022	3.158
	A	3.380	3.169

Table 4.6. Normalized dose values for comparisons of PCS and AcurosPT against the measured for SOBP at 20cm WET.

SOBP 20cm WET	PCS/ Measured	(±) % Error	AcurosPT/ Measured	(±) % Error	Measured
2x2x6	102.75	2.75	98.65	-1.35	100
3x3x6	102.33	2.33	98.98	-1.02	100
5x5x6	99.02	-0.98	100.96	0.96	100
10x10x6	96.80	3.20	102.69	2.69	100
20x20x6	95.87	4.13	106.96	6.96	100

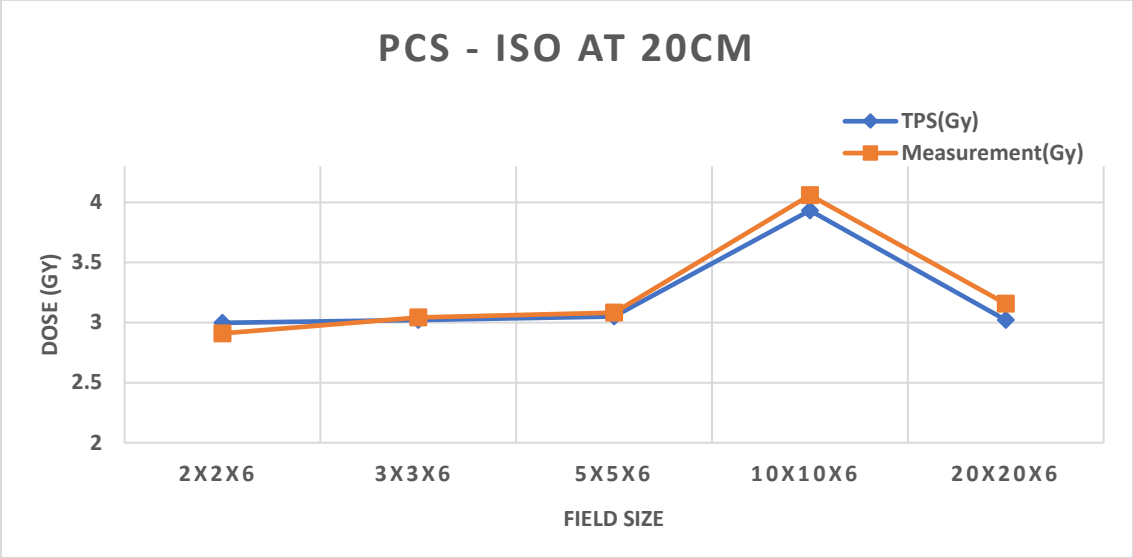

Fig.4.19. Dose comparison in PCS algorithm with an isocenter at 20cm WET for different fields in open conditions.

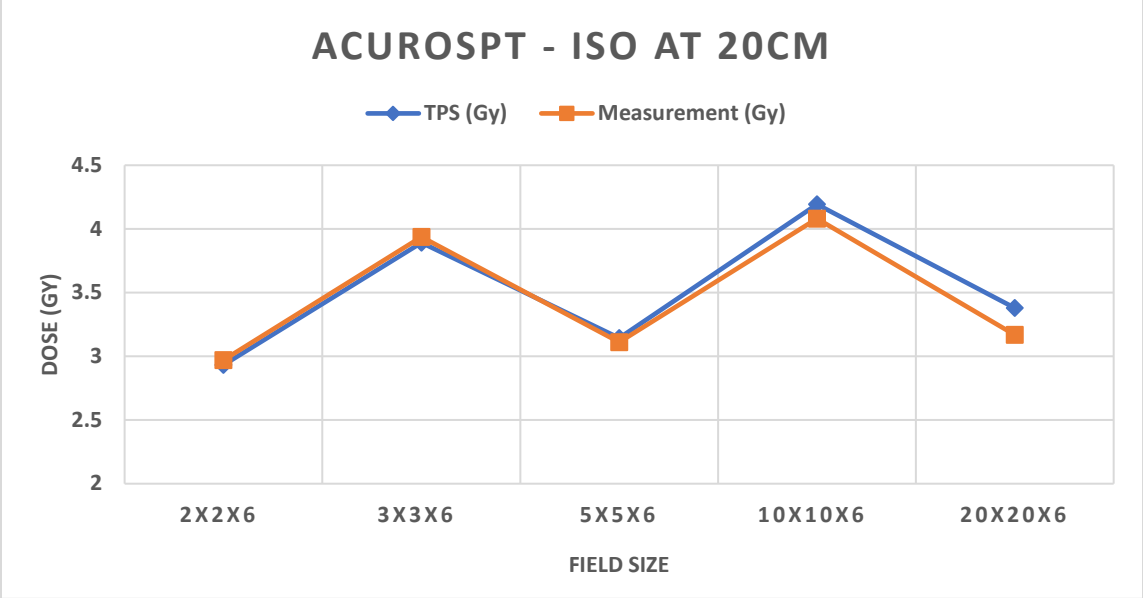

Fig.4.20. Dose comparison in AcurosPT algorithm with an isocenter at 20cm WET for different fields in open conditions.

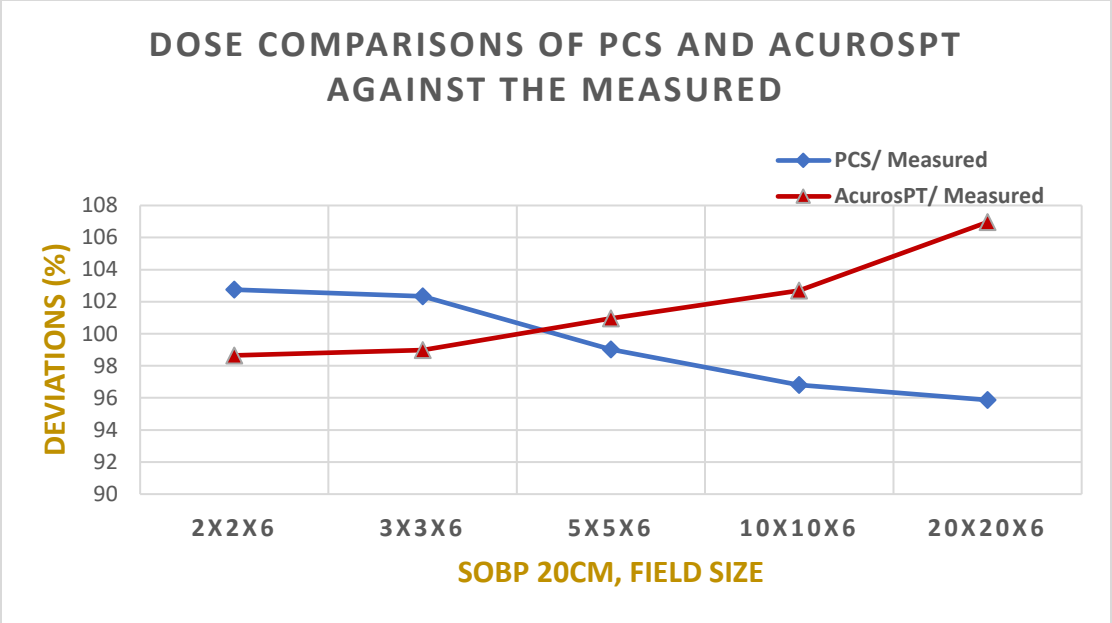

Fig.4.21. Comparison of measured doses against those in of P and A plans for ISO at 20cm WET.

4.4 Conclusion

This study that the dosimetry output of small scanning proton fields (especially at superficial depth) in Eclipse 15.6 is inadequately modeled the halo effect, contributed by the low dose region off central axis, or tail regions of Gaussian-distributed dose model, of the proton beam. In AcurosPT, the relatively elevated lateral dose tails extend beyond the actual region, so although it still shows lightly lower computed doses in very small fields, higher computed doses are seen in large proton fields. In contrast, the underdose are seen in large field computed by single-Gaussian modeled PCS algorithm. Basically, we have one Gaussian model for the PCS beam dose distribution with missing dose tails in its outer regions. Therefore, for smaller fields the part of the tail, contribution will be missing to the dose, and that is why we have as much as 7.53% less dose for 2cm field with 25cm air gap and the use of range shifter. This underdose output would have a clinical impact in cases of skin cancer or shallow small breast cancers.

The situation is opposite for the bigger fields – 20cm. In AcurosPT, the tail will raise a little bit considering the scatter, which is better than in single gaussian (PCS), and for bigger fields they will combine. The increase of the dose in AcurosPT up to 7.40% (20cm field at 15cm air gap with a range shifter) is as a result of these tails. As we explained, AcurosPT does somewhat better because the tail is higher in the model.

Measurements show big differences between two algorithms especially for small and large fields in deep and shallower depths.

In small fields (2cm) in deeper depth AcurosPT output is 4.11% less than PCS, and in shallower depth PCS delivers up to 8.07% more dose than AcurosPT.

In big fields (10cm and 20cm) in both deep and shallower depth, AcurosPT delivers more dose than PCS. In deeper depth targets (20cm field) the difference is 11.09% and in shallower depth targets (15cm air gap) the difference is 12.94%.

Further investigation of Halo effect could include measuring the dose output with a EBT3 Gafchromic film and comparing the results that we have with ion chamber. Another useful way to measure the effect would be to use water tanks instead of solid water phantoms, use of 2.28cm, 3.42cm WET range shifters and compare the discrepancies between TPS and the dose delivered.

Chapter 5: References

[1] Mikaela Dell'Oro, Michala Short, Puthenparampil Wilson, et al., "Clinical Limitations of photon, Proton and Carbon Ion Therapy for Pancreatic Cancer", 2020, doi.org/10.3390/cancers12010163

[2] Seo Hyun Park, MS, Jin Oh Kang, MD, "Basics of particle therapy I: physics", Radiation Oncol J. 2011 Sep, doi: 10.3857/roj.2011.29.3.135

[3] Podgorsak, Ervin B. Radiation Physics for Medical Physicists. Springer, 2018.

[4] Britt H. Tonneson, MD, Roper St. Francis Heart, "Radiation physics", 2011, J Vasc Surg 2011;53:6S-8S.) doi: 10.1016/j.jvs.2010.05.138

[5] Shen J, Lentz JM, Hu Y, et al. Using field size factors to characterize the in-air fluence of a proton machine with a range shifter. Radiat Oncol. 2017; 12:52

[6] Both S, et al. Development and clinical implementation of a universal bolus to maintain spot size during delivery of base of skull pencil beam scanning proton therapy. Int J Radiat Oncol Biol Phys. 2014;90(1):79–84.

[7] University of Florida, Radiation Safety Short Course Study Guide - RSSC Administrative Structure Radiation Control Program, chpt: 2, 2011, pp 9-14. https://webfiles.ehs.ufl.edu/rssc_stdy_chp_2.pdf

[8] John F. Dicello, Ph.D., "Absorption Characteristics of Protons and Photons in Tissue", 2007, PMID: 17668948 doi: 10.1177/15330346070060S404.

[9] Dingfelder M, Inokuti M, Paretzke HG. Inelastic-collision cross sections of liquid water for interactions of energetic protons. Radiat Phys Chem 2000; 59:255-75.

[10] Newhauser, W. "International Commission on Radiation Units and Measurements Report 78: Prescribing, Recording and Reporting Proton-Beam Therapy." Radiation Protection Dosimetry, vol. 133, no. 1, 2009, pp. 60–62., doi:10.1093/rpd/ncp005.

[11] Bragg W, Kleeman R. On the alpha particles of radium and their loss of range in
passing through various atoms and molecules. Phil. Mag. 1905; 10:318–40.

[12] J. Deasy, ICRU Report 49, stopping powers and ranges for protons and alpha particles, Wiley Online Library, 1994.

[13] Paganetti, Harald. “Range Uncertainties in Proton Therapy and the Role of Monte Carlo Simulations.” Physics in Medicine and Biology, vol. 57, no. 11, 2012, doi:10.1088/0031-9155/57/11/r99.

[14] Hans Breuer, Berend J. Smith, “Proton Therapy and Radiosurgery” Springer-Verlag Berlin Heidelberg (2000), pp.25-35, doi: 10.1007/978-3-662-04301-1

[15] Luther W. Brady, Carlos A. Perez, et al., “Perez & Brady’s Principles and Practice of Radiation Oncology” Seventh Edition, pp. 839-840, 2018.

[16] Harald Paganetti, “Proton Therapy Physics”, pp. 20-57, 2012, doi: 978-1-4398-3645-3

[17] Gottschalk, Bernard, et al. “On the Nuclear Halo of a Proton Pencil Beam Stopping in Water.” Physics in Medicine and Biology, vol. 60, no. 14, 2015, pp. 5627–5654., doi:10.1088/0031-9155/60/14/5627.

[18] Highland, Virgil L. “Some Practical Remarks on Multiple Scattering.” Nuclear Instruments and Methods, vol. 129, no. 2, 1975, pp. 497–499., doi:10.1016/0029-554x(75)90743-0.

[19] Bernard Gottschalk, “Techniques of Proton Radiotherapy (07) Nuclear Reactions”, 2011

[20] Stephen M. Seltzer. An assessment of the role of charged secondaries from nonelastic nuclear interactions by therapy proton beams in water. NIST technical note NISTIR 5221 (1993). Available from the National Technical Information Service, NTIS, U.S. Department of Commerce, Springfield, VA 22161.

[21] Hsiao-Ming Lu, Ph.D., Jay Flanz, Ph.D., Harald Paganetti, Ph.D. “Physics of Particle Beams”, PTCOG 53 Education Session, Shanghai, 2014 http://ptcog.ch/archive/conference_p&t&v/PTCOG53/PresentationsEW/PTCOG53_Lu.pdf

[22] E. Pedroni, S. Scheib, T. B¨ohringer, A. Coray, M. Grossmann, S. Lin and A. Lomax, ‘Experimental characterization and physical modeling of the dose distribution of scanned proton pencil beams,’ Phys. Med. Biol. 50 (2005) 541-561.

[23] T.P.Wangler, K.R.Crandall, “Beam Halo in Proton Linac Beams”, vol. 1, 2, pub.: eConf C000821 (2000) TU202.

[24] J. Hall, Amato J. Giaccia, “Radiobiology for the radiologist”, Eighth edition, 20419, pp.808, doi.org/10.1667/RR0771.1.

[25] Massachusetts General Hospital, Department of Radiation Oncology, Physics Division, Techniques of Proton Radiotherapy (01) Introduction", 2021 https://gray.mgh.harvard.edu/attachments/article/337/Techniques%20of%20Proton%20Radiotherapy%20(10)%20Bragg%20Peak.pdf

[26] Michael G. Stabin, PhD, "Fundamentals of Nuclear Medicine Dosimetry", 2008, pp. 183-189, doi: 10.1007/978-0-387-74579-4

[27] Harald Paganetti, PH.D., Andrzej Niemierko, PH.D.,Marek Ancukiewicz, PH.D., "Relative Biological Effectiveness (RBE) values for proton Beam therapy" Vol. 53, No. 2, pp. 407–421, 2002, doi.10.1016/S0360-3016(02)02754-2

[28] Yusuke Fuji Toru Umekawa, Ph.D., Masumi Umezawa, "Industry-Academia Collaboration and Intellectual Property Creation in Development of Particle Beam Therapy System", 2019 vol.68 No.3

[29] Tom Depuydt, "Proton therapy technology in the clinic", 2018, doi:10.1177/0146645318756252

[30] Harald Paganetti and Thomas Bortfeld "Proton Beam Radiotherapy -The State of the Art[1]", pp.16-21, 2005, doi:10.1007/s12194-017-0428-z.

[31] Andrew J. Wroe, Jerry D. Slater, James M. Slater, "The Physics of Protons for Patient Treatment", pp.1-5, 2012,

[32] Trofimov A, Bortfeld T. 2003. Optimization of Beam Parameters and Treatment Planning for Intensity Modulated Proton Therapy. Technology in Cancer Research & Treatment 2:437-444.

[33] Jatinder Saini, Erik Traneus, Dominic Maes, et al., "Advanced Proton Beam Dosimetry Part I: review and performance evaluation of dose calculation algorithms", 2018, doi: 10.21037/tlcr.2018.04.05

[34] International Commission on Radiation Units and Measurements. Report No. 78.
Bethesda, MD: International Commission on Radiation Units and Measurements. 2007. Prescribing, Recording, and Reporting Proton-Beam Therapy.

[35] Witold Matysiak, Daniel Yeung, Roelf Slopsema, Zuofeng Li, "Evaluation of the
range shifter model for proton pencil-beam scanning for the Eclipse v.11 treatment
planning system", Journal of Applied Clinical Medical Physics, Vol. 17, No. 2,

[36] Jatinder Saini1, Erik Traneus, Dominic Maes, Rajesh Regmi, Stephen R. Bowen,
Charles Bloch, Tony Wong. Transl Lung Cancer Res 2018;7(2):171-17

[37] S. B. Harrabi, M.D., N. Bougatf, A. Mohr, M.D., “Dosimetric advantages of proton therapy over conventional radiotherapy with photons in young patients and adults with low-grade glioma”, 2016, doi: 10.1007/s00066-016-1005-9

[38] PTW, The Dosimetry Company, RW3 Slab Phantom
https://www.ptwdosimetry.com/en/products/rw3-slab-phantom/

[39] PTW, The Dosimetry Company “RADIATION MEDICINE QA, SOLUTIONS”
https://www.ptwdosimetry.com/en/products/octavius-detector-1500xdr/